Development and Analysis of Hybrid Additive Manufacturing Process

M.Tech. Thesis

By

Siddhant S Barman

DISCIPLINE OF MECHANICAL ENGINEERING

INDIAN INSTITUTE OF TECHNOLOGY INDORE

May, 2024

Development and Analysis of Hybrid Additive Manufacturing Process

A THESIS

Submitted in partial fulfillment of the requirements for the award of the degree
of
Master of Technology
in
Mechanical Engineering
with specialization in
Advanced Manufacturing

by

Siddhant S Barman

DISCIPLINE OF MECHANICAL ENGINEERING
INDIAN INSTITUTE OF TECHNOLOGY INDORE

May, 2024

INDIAN INSTITUTE OF TECHNOLOGY INDORE

CANDIDATE'S DECLARATION

I hereby certify that the work which is being presented in the thesis **Development and Analysis of Hybrid Additive Manufacturing Process** in the partial fulfillment of the requirements for the award of the degree of **MASTER OF TECHNOLOGY** and submitted in the **DISCIPLINE OF MECHANICAL ENGINEERING, Indian Institute of Technology Indore**, is an authentic record of my own work carried out during the time period from July, 2023 to May, 2024 under the supervision of Dr. Yuvraj Kumar Madhukar, Assistant Professor in the Department of Mechanical Engineering.

The matter presented in this thesis has not been submitted by me for the award of any other degree of this or any other institute.

Siddhant S Barman

(Siddhant S Barman)

This is to certify that the above statement made by the candidate is correct to the best of my/our knowledge.

Dr. Yuvraj Kumar Madhukar 25/05/24

(Dr. Yuvraj Kumar Madhukar)

Siddhant S Barman has successfully given his M.Tech. Oral Examination held on **31.5.2024.**

Signature of Supervisor of M.Tech. thesis — Convener, DPGC

Date: — Date:

ACKNOWLEDGEMENTS

I am very thankful to **Dr. Yuvraj Kumar Madhukar** for trusting me and providing me with the opportunity to perform this research work under his valuable supervision. He motivated me and gave his great ideas with important key points for understanding the depth of a subject. His suggestions and comments helped me to modify the research work in a positive direction. I take my deep sense of respect and gratitude for his guidance and lessons.

My gratitude is extended to the committee members, **Prof. Satyajit Chatterjee, Prof. Kazi Sabiruddin, Dr. Girish Verma and Dr. Ashish Rajak** for their valuable guidance, suggestions and support in this research work.

I express my sincere gratitude to PhD scholar, Dr. Anas Ullah Khan, Mr. Rajendra Goud and Mr. Arun Kumar Singh for their technical assistance in my project.

I would like to express my thanks to Mr. Umakant Sharma and Mr. Satish Kaushal of Central Workshop, IIT Indore for their assistance in making the linear stage.

The Discipline of Mechanical Engineering, IIT Indore is gratefully acknowledged for giving me an opportunity to carry out my M.Tech and needed thesis work. A heartfelt thanks to my friends, Hrishikesh Meshram and Rishabh Verma for their help and support for carrying out this project work.

Lastly, I would like to thank almighty God, my parents and my sister who always gave me strength, motivation, confidence and love to successfully perform all tasks of my life.

Siddhant S Barman

Abstract

Additive manufacturing (AM) is the process of joining materials to make parts or objects from 3D model data, usually layer upon layer, as opposed to subtractive manufacturing methodologies. The additive manufacturing is also called rapid prototyping, 3D printing etc. It can produce complex geometrical net or near-net shapes and ready to use products. Earlier it was used for fast fabrication of prototypes to check shape, size and functions, as the AM has freedom in part design and also the capability to reduce the production time, waste and cost. Nowadays, additive manufacturing is widely used in automotive, aerospace, biomedical, defence, electronics and construction etc. sectors. Direct Energy Deposition (DED) is a series of several similar metal 3D printing technologies that creates parts by melting and fusing material as it is deposited. The combination of an electric arc as heat source and wire as feedstock is referred to as wire arc additive manufacturing (WAAM). The arc-based additive manufacturing processes are growing fastly in the manufacturing industry as it can fabricate metal components in lower cost with shorter production time. The various WAAM processes are gas metal arc welding (GMAW), gas tungsten arc welding (GTAW), plasma arc welding (PAW). WAAM is better than other AM technologies as it provides better material deposition, lower energy consumption and improved energy efficiency. The combination of laser as heat source and wire as a feed stock is referred to as wire laser additive manufacturing (WLAM). The objective of the study is to compare Wire TIG Additive Manufacturing, Wire MIG Additive Manufacturing, Wire Laser Additive Manufacturing, Laser-TIG Hybrid Additive Manufacturing and MIG-TIG Hybrid Additive Manufacturing under a common set of parameters and material and to identify the efficient process based on energy utilization, bead quality (height, width and uniformity) and material property (hardness).

TABLE OF CONTENTS

List of Figures

List of Tables

Chapter 1
Introduction

1.1 Additive Manufacturing

Additive manufacturing (AM) is the process of joining materials to make parts or objects from 3D model data, usually layer upon layer, as opposed to subtractive manufacturing methodologies. The additive manufacturing is also called rapid prototyping, 3D printing etc. It can produce complex geometrical net or near-net shapes and ready to use products. Earlier it was used for fast fabrication of prototypes to check shape, size and functions, as the AM has freedom in part design and also the capability to reduce the production time, waste and cost [1]. Nowadays, additive manufacturing is widely used in automotive, aerospace, biomedical, defence, electronics and construction etc. sectors [2]. Also, the additive manufacturing is expected to be a key technology in the fourth industrial revolution, i.e. industry 4.0 [3]. There are a lot of material deposition techniques which divide into several parts-

- Powder Bed Fusion
- Material extrusion
- Vat photopolymerization
- Direct Energy Deposition
- Material jetting
- Binder jetting.
- Laminated object manufacturing (LOM)

The above discussed AM includes the use of metal and its alloys, ceramics, polymer, composites, fibres, woods etc. the broad range of work material also makes additive manufacturing important.

1.2 Wire Arc Additive Manufacturing (WAAM)

The arc-based additive manufacturing processes are growing rapidly in the manufacturing industry as it can fabricate metal components in lower cost with shorter production time [4]. Direct Energy Deposition (DED) is a series of several similar metal 3D printing technologies that creates parts by melting and fusing material as it is deposited. The combination of an electric arc as heat source and wire as feedstock is referred to as wire arc additive manufacturing (WAAM). WAAM consist welding power source, torches and wire feeding systems, as shown in Figure 1. The material is deposited by giving the motion to the torch either by using CNC gantries or by robotic systems. This tool-less method is capable of producing fully dense part in less time.

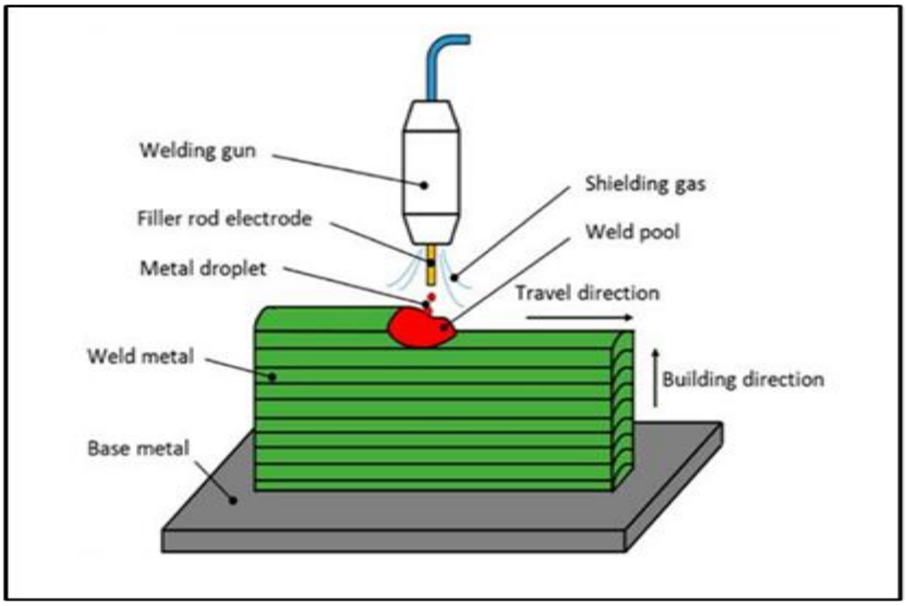

Fig. 1: Wire Arc Additive Manufacturing [4]

Although WAAM has many advantages, few reasons are there which limits its applications:

- Heating involved in welding processes it induces residual stresses and distortion in manufactured parts [5].
- The fabricated parts relatively poor, when compared with the laser based process, which requires significant post- processing for application acceptance [6].
- The presence of a large number of voids between deposited layers [7].
- Automation in the field of additive manufacturing is not developed [8].
- The absence of process monitoring and control during deposition limits its application[8]

Generally, the deposition of material in wire + arc additive manufacturing (WAAM) is done with the help of

- Gas metal arc welding (GMAW)
- Gas tungsten arc welding (GTAW)
- Plasma arc welding (PAW)

1.2.1 WAAM parts example

The WAAM deposited bead height is generally 1 to 2 mm. The presence of surface roughness or waviness of bead required further finishing. Due to limited research WAAM is suitable for low to medium complex parts. Also, it has limitations means it is not suitable for small scale parts. Figure 2a shows 1.2 m wing spar, which was deposited by plasma arc welding. Figure 2b shows the ship propeller of diameter 1.3 m; it was used in the ship after post-processing. Figure 2c shows the wing for the wing tunnel testing. It was developed to reduce the testing time as it can be produced in a few hours. Figure 2d shows the truncated cone with a wall thickness of 2.5 mm. All the above discussed WAAM parts show the capability of the process.

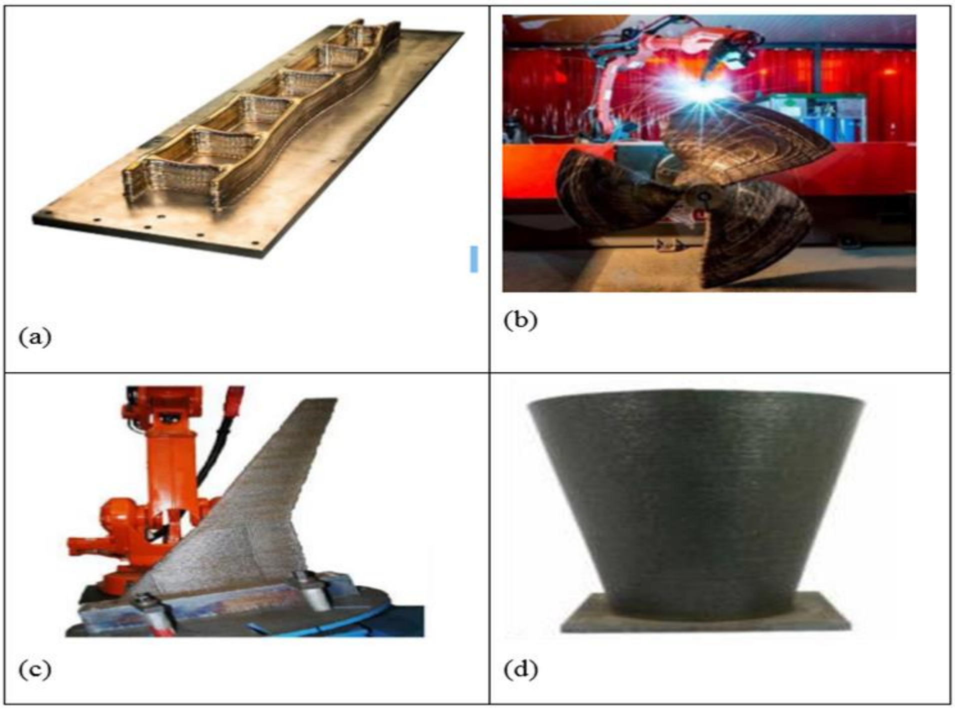

Fig. 2: WAAM Parts [9]

1.2.2 Comparison of various WAAM Techniques [10]

Table 1: WAAM types based on deposition technique and its characteristics

WAAM type	Power source	Characteristics
GTAW-based	GTAW	Non-consumable electrode. Separate wire feed process. deposition rate: 1-2 kg/hour. Wire and torch rotation is needed.
GMAW-based	GMAW	Consumable wire electrode. deposition rate 3-4 kg/hour. Poor arc stability, spatter.
PAW-based	Plasma	Non-consumable electrode. Separate wire feed process. deposition rate 2-4 kg/hour. Wire and torch rotation is needed.

1.3 Gas Tungsten Arc Welding (GTAW)

Gas tungsten arc welding (GTAW), also known as tungsten inert gas welding. It is an arc-based welding process which uses non-consumable tungsten electrode for the generation of arc, as shown in Figure 3. The filler rod is used to fill the gap. The weld bead is protected from oxidation by an inert gas (argon). It is useful in many applications due to its capability to promote all three types of welding, namely autogenous, homogeneous and heterogeneous. Here autogenous, homogeneous and heterogeneous welding process is referring to the process where no-filler material, the filler similar to the base material, and the filler different from the base material is used, respectively.

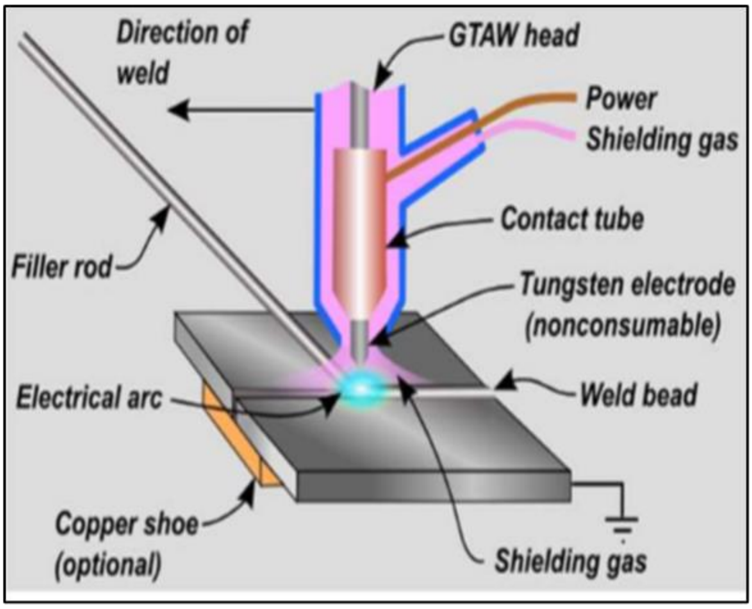

Fig. 3: GTAW Schematic [11]

1.4 Wire Laser Additive Manufacturing (WLAM)

Laser Wire-Feed Metal Additive Manufacturing (LWAM) is a process that utilizes a laser to heat and melt a metallic alloy wire, which is then precisely positioned on a substrate, or previous layer, to build a three-dimensional metal part. LWAM utilizes a metal wire feedstock and a laser to create a molten pool. A protective shield of gas is used to keep the material being deposited uncontaminated. The process involves melting a wire with an energy source to form a liquid bead, which is then added, layer by layer, to create the final product LWAM technology offers several advantages, such as high speed, cost effectiveness, precision control, and the ability to create complex geometries with near-net shape features and improved metallurgical properties [12].

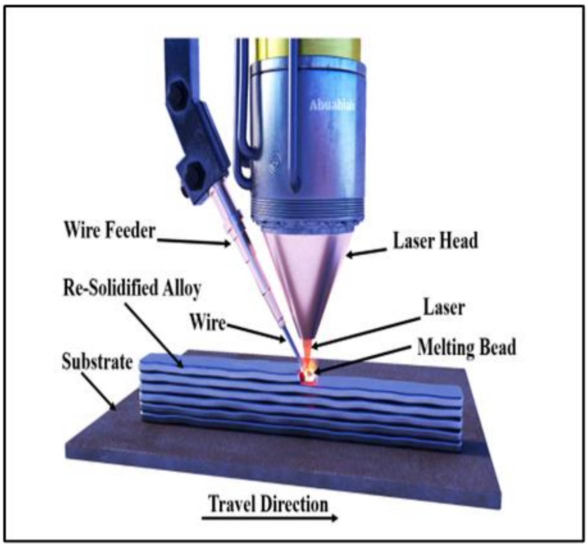

Fig. 4: Diagrammatic representation of the LWAM's bead deposition mechanism [12]

1.5 Gas Metal Arc Welding (GMAW):

GMAW, also known as MIG (Metal Inert Gas) welding, is a widely used WAAM process. It employs a consumable wire electrode and a shielding gas to protect the arc and molten pool from atmospheric contamination. GMAW-WAAM offers good control over the deposition rate and is commonly used for fabricating large-scale parts [13].

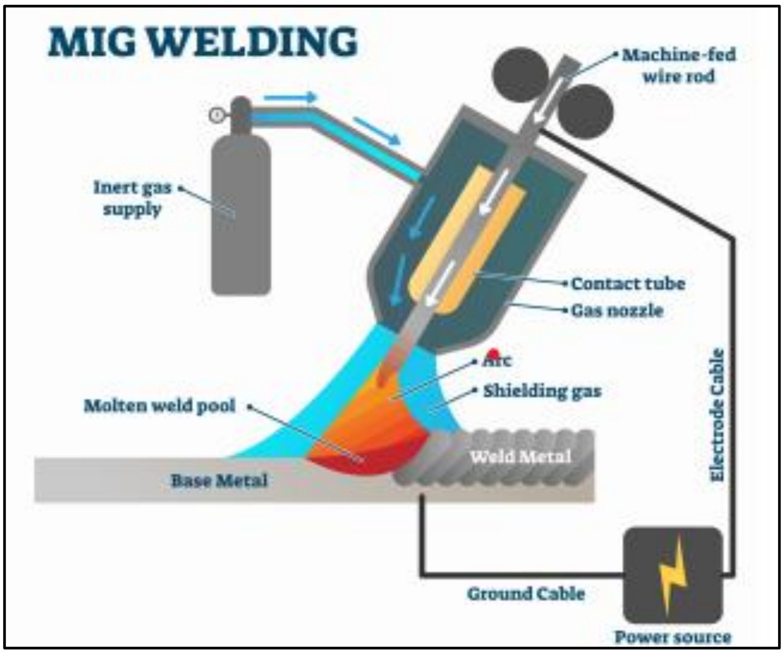

Fig. 5: GMAW Schematic [13]

1.6 Laser-TIG Hybrid Welding (LTHW)

LTHW uses both laser and TIG for welding. The wire is fed from the spool and laser and TIG together generate heat to melt the wire and it results in formation of the weld bead. The weld bead produced in this case has better metallurgical conditions, low distortion and improved gap bridging.

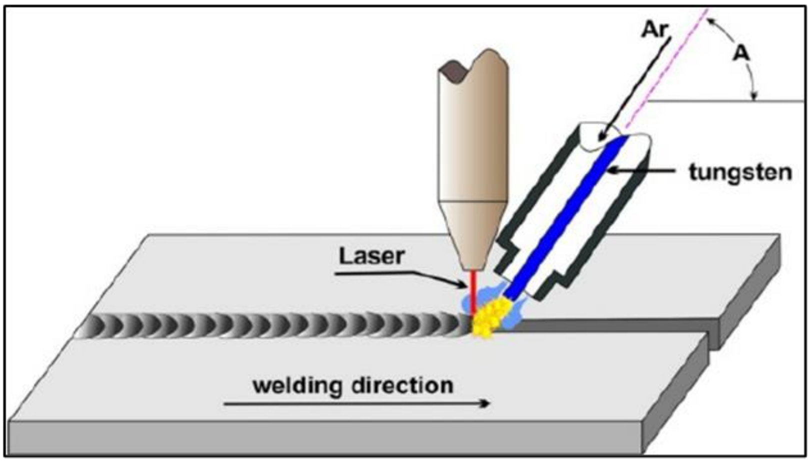

Fig. 6: Schematic of Laser-TIG Hybrid Welding [14]

1.7 MIG-TIG Hybrid Welding (MTHW)

MTHW uses both MIG and TIG as heating source to melt the wire which is being fed automatically from the spool. This results in the formation of the weld bead. The weld bead produced in this case has better metallurgical conditions.

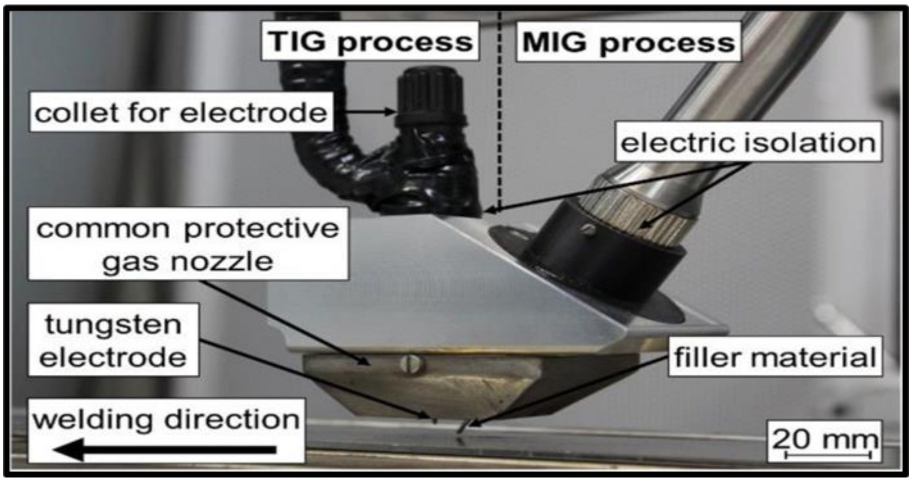

Fig. 7: MIG-TIG Hybrid Welding [15]

Chapter 2
Literature Review and objective formulation

2.1 Additive Manufacturing Process (WAAM)

Wu et al. discussed the various aspects of arc-based additive manufacturing (tungsten inert gas welding, gas metal arc welding, plasma arc welding, etc.) including mechanical, structural and microstructural properties. They also addressed that various defects commonly observed in the process such as porosity, residual stresses and cracking, etc. are due to the variation in thermal characteristics during the deposition. They found that the online temperature and heat input can be controlled in a range to get the desired microstructure and mechanical properties. Further, the changing in arc parameters and metal transfer at the same time makes the process stable and defect-free [10].

Williams et al. reported that the wire arc additive manufacturing (WAAM) process could replace current manufacturing trends where blooms and billets are used for manufacturing of components. They used high-pressure interpass rolling to reduce residual stresses. However, there are associated limitations to achieve complex geometry and make it defect-free. They suggested that realtime temperature monitoring and feedback systems could minimise these issues [9].

Herzog et al. reviewed the influence of the thermal cycle on the different properties of the additively manufactured parts for laser beam, electron beam and plasma beam process. They also define the relation between process, microstructure and properties. The effect of thermal cycle and high cooling rates on grain structure are analysed [16].

Tapia et al. discussed the various temperature sensors that can be utilised for temperature measurement and real-time controlling of AM. The determination of material emissivity is very difficult, and this can be lead to inaccurate temperature measurement. Also, the AM setups are not equipped with the customised inbuilt monitoring sensor, which limits the process monitoring and real-time controlling [17].

Pan et al. discussed the recent research in additive manufacturing monitoring and controlling. They find the need for automation of the process. Also, there is further research in process control, and optimisation is required to control residual stress and distortion [8].

2.2 Tungsten Inert Gas Welding

Tungsten Inert Gas (TIG) or Gas Tungsten Arc Welding (GTAW) is a traditional method of welding for quality products. It is useful in many applications due to its capability to promote all three types of welding, namely autogenous, homogeneous and heterogeneous. Here this autogenous, homogeneous and heterogeneous welding process is referring to the process where no-filler material, the filler similar to the base material, and the filler different from the base material is used, respectively. Many researchers have widely studied this welding process for the welding of a broad range of material, including metals and alloys, to explore the various advantages and the process applicability [18-22]. This non-consumable electrode process is found useful in many other applications such as surface hardening, melting, alloying, cladding, additive manufacturing, etc [23-31].

Kumar et al. performed surface modification in AISI 4340 steel by multi-pass TIG arcing process. They studied the effect of process parameters by varying arcing current and travel speed while keeping arc voltage constant at 10.5 ± 1.0 V. They found that the process improved the surface hardness and other mechanical properties. The magnitude of change in the property was dependent on the heat input [24].

Mustafa et al. modified the steel substrate surface with TIG welding. They reported that the alloying of SiC on the steel substrate could vary the hardness between 670 and 1165 Hv. They also observed that with high heat input, there is a difference between surface and inner part properties which induces residual stresses [32].

Orlowicz et al. performed the surface hardening of nodular cast iron by TIG remelting. The TIG current and scanning speed was varied in the range of 50– 300 A and 200–800 mm/min, respectively. They observed that the surface hardness reduces with the increase of arc current. However, it increased with an increase in scanning speed for all current intensity studied. The increase in hardness due to fast solidification of superficial regions contributes to the crystallisation of cementite eutectic which transformed austenite present in the eutectic into partly martensite. They also observed that the remelting depth and width both increased with the increase of current intensity for all scanning speed [33].

Karamis et al. employed TIG melting and controlled chilling process to eliminate the graphite phase nodule from the cast iron. They found chilling process could not eliminate the graphite phases from nodular cast iron while an almost nodule-free surface was obtained by the TIG melting process. They reported that the depth and width of the change in microstructure could be controlled more effectively with an automated system [34].

Lv et al. compared the cladding of hot and cold copper wire on the steel substrate. An additional TIG arc was used for heating of the wire. They found that below 240 A the spreadability of hot wire was better than the cold wire. They also found that the cladding hardness improved with the increase of current and dependent on Fe content [35].

Guijun et al. used the laser for cladding purposes and concluded that the dilution of the powder is mainly dependent on the temperature of the weld pool. Also, the dimension of the clad layer is dependent on the temperature of the weld pool [36].

Liberini et al. used wire arc additive manufacturing (WAAM) to deposit successive layers of materials on a low carbon steel substrate. The filler material used was ER70S-6 steel, and the process parameters were varied to understand their effect on the final product's mechanical characteristics. The experimental campaign included macrographic observations, micrographic observations, and Vickers microhardness tests. The samples were analyzed using scanning electron microscopy (SEM) and confocal microscopy to study the microstructure and surface characteristics. The study of samples produced by Wire Arc Additive Manufacturing technology led to several conclusions: the cooling curve had a preeminent effect on the product microstructure, which was not substantially affected by process parameters, three different zones were observed in all the samples: lower zone with ferritic structure, middle zone with equiaxed grains of ferrite, and upper zone with a lamellar bainitic structure, the difference in the three microstructures was attributed to the different thermal history experienced by the welding beads deposited, with the upper zone affected by stronger thermal shock, Vickers microhardness values confirmed the different microstructures found in the samples. The study suggested a strategy to obtain a ferrite/bainite structure by alternating cooling cycles with water or oil between the deposition of weld beads [37].

2.4 Wire Metal Inert Gas (MIG) Additive Manufacturing

Panchenko et al. fabricated parts using MIG arc additive manufacturing with Al7075 wire in 15 layers. Enhanced microstructural characteristics achieved with MIG arc additive manufacturing. Improved mechanical properties and fatigue resistance were observed in Al7075 alloy through electron beam melting. Variation in microhardness and fatigue performance across different regions of fabricated parts [38].

Liao et al. used pulsed MIG welding in a water tank with a water depth of 200 mm to study the of welding speed on welding process stability, microstructure and.pdf" involves investigating the influence mechanism of welding speed on welding process stability, microstructure, and mechanical properties of SUS304 LDU-PMIG weldments. The study found that with the increase of welding speed from 9.0 mm/s to 16.2 mm/s, the welding process stability first improved and then deteriorated. The weldment obtained at 12.6 mm/s exhibited the highest microhardness, tensile strength, and elongation, which achieved 70.0%, 92.3%, and 61.6% of the base metal. The increase of welding speed led to the S-ferrite morphological evolution from skeletal to lath, which promoted the transformation from brittleness to ductility in the weld mechanical performance. The proportions of small-size grains (less than 10 um) and low-angle grain boundaries (2-15°) first increased and then decreased, which determined the same variation trend in the comprehensive mechanical performance of weldments [39].

Khan et al. discussed a study on in-situ temperature monitoring and feedback control in the gas tungsten arc welding (GTAW) process. The system uses a ratio pyrometer for temperature monitoring and a data acquisition system to bridge communication between a computer and the GTAW power source. The effects of controlled temperature on the properties of deposited beads, such as micro-indentation hardness and bead geometry were studied. The outcomes of the study demonstrate successful temperature control within a broad range of 400–1600°C, with marginal errors in different experimental conditions. The controlled temperature affects the bead properties, with higher setpoint temperatures leading to lesser hardness and vice versa [40].

Oua et al. developed a three-dimensional heat transfer and fluid flow model for wire arc additive manufacturing to calculate fusion zone geometries, cooling rates, and solidification parameters. Little difference is observed in distribution at different distances from the arc center. Small convection loop in front and larger loop in rear of molten pool and higher surface tension gradient near front and lower in rear correlates with velocities [41].

2.4 Wire Laser Additive Manufacturing

Zhao et al. fabricated Ni/WC composite coatings using laser hot-wire deposition. The laser hot-wire deposition system consisted of a 2 kW Nd:YAG laser, a power source, a wire feeder, and a 3D platform. Carbon steel was used as the substrate, and a tubular cored wire consisting of nickel sheath and mixed powders including eutectoid-structured WC/W2C particles and other alloying elements was used for the deposition. The optimal parameters including laser power, scanning speed, wire feeding rate, and heating current were applied to fabricate the coatings. The samples were evaluated by scanning electron microscope, EBSD mapping, dry sliding wear tester, and Vicker microhardness tester. The outcomes of the study showed that the laser hot-wire deposition method successfully synthesized finely dispersed WC particles, resulting in improved coating hardness and wear resistance. The retained particles distributed uniformly with a volume fraction of 29%, and the coating exhibited a microhardness of 1100 HV0.2, which was higher than that of the substrate. The wear rate of the coating was reduced by 60% compared to the substrate, indicating improved wear resistance. The study suggests that the laser hot-wire deposition method is a promising approach for fabricating Ni/WC composite coatings with improved properties [42].

Baghdadchi et al. used wire laser metal deposition additive manufacturing to manufacture duplex stainless steel components. Microstructure, chemical composition, and mechanical properties of the components at each stage were evaluated and tested. The study found that the microstructure of the components can be controlled by adjusting the heat input and wire pre-heating, and implementing a cooling system to prevent an increase in temperature that would decrease productivity. The mechanical properties of the components can be improved by heat treatment, which homogenizes the microstructure and removes nitrides [43].

Naksuk et al. utilized a hot-wire laser welding process with the help of a KUKA robot's robotic welding system. The welding movement relative to the substrate was generated using a six-degree-of-freedom KUKA industrial robot arm. The study measured the Vickers microhardness values for the hot-wire laser welding technique. The study examined the levels of porosity in the welded parts. The root of porosity was found to be the portion of root volume absorbed by the surrounding air, nitrogen, oxygen, hydrogen, and contamination in the melting pool. Factors such as bulk density, root growth rate, availability of inert gas, and temperature influenced the level of porosity. The study also investigated the mechanical properties of the welded parts, including tensile stress, tensile strength, elongation at break, thickness, and width [44].

Zapata et al. used a laser metal deposition system with coaxial wire feeding to investigate the cause-effect relationships between process parameters and the resulting geometric properties for wire-based coaxial laser metal deposition. The study focused on the deposition of near net shape parts using laser-based processes. The process parameters, such as laser power, wire speed and traverse speed were varied to identify suitable parameter windows for the deposition of aluminium and stainless steel. The geometric properties of the deposited beads, such as height and width, were measured using a 3D profilometer. The data obtained from the experiments were analysed to determine the relationships between the process parameters and the geometric properties. The outcomes of the research include the identification of process windows for the deposition of aluminium and stainless steel. The process maps show the suitable parameter ranges for achieving defect-free deposition. The research also analysed the formation mechanisms of process defects, such as stubbing and dripping, and proposed methods to reduce their occurrence [45].

Chuang Guo and Jiangqi Long developed a three-dimensional numerical model to simulate the heat transfer and geometric morphology of multi-channel deposition in laser wire additive manufacturing. The outcomes of the study showed that the lap ratio significantly affected the geometric morphology of the deposited parts. At a lap ratio of 10%, the morphology was uneven, while at 20%, the flatness was the best. However, at a lap ratio of 30%, the morphology formed a slope. Based on the evaluation of surface flatness, the optimal lap ratio was determined to be 20%, which is crucial for subsequent additive manufacturing processes [46].

He et al. used a coaxial double laser metal-wire deposition (LMwD) setup to deposit Ti6Al4V alloy. The setup involved an ytterbium fiber laser system with two coaxially mounted irradiated laser torches and a 1.0 mm diameter Ti6Al4V wire on the Ti6Al4V base metal. The process parameters were optimized based on previous experiments, with a laser power of 1000 W, a head feed speed of 500 mm/min, and a wire feed speed of 191 mm/min. The microstructure was observed using scanning electron microscopy (SEM) and the element composition was explored with energy-dispersive spectroscopy (EDS). X-ray diffraction (XRD) was performed to investigate the element composition. The temperature and residual stress distribution of the substrate were simulated and calculated using Simufact software. The study found that the as-built single-bead samples displayed smooth morphology with a high-quality surface and almost no contamination. However, the microstructure of the outer edge area of the single-bead exhibited a thin oxide layer. The thin-wall as-built component displayed worse oxidation resistance, with limited argon gas circulation resulting in color changes and reduced gas protection. The study also conducted a simulation of temperature and residual stress distribution to further clarify the microstructure characteristics [47].

Ding et al. used a laser coaxial wire feeding additive manufacturing technique to fabricate 4043 Al alloy in a vacuum environment. The study aims to understand the impact of ambient pressure on bead shape, microstructure, and corrosion behaviour. The results indicate that lower ambient pressure results in wider, smoother, and better-wetted bead shapes, suggesting improved forming at lower pressures. Microstructural analysis reveals reduced porosity and improved cellular structure at lower pressures. X-ray diffraction patterns show a decrease in Al phase intensity and lower microhardness at higher pressures. Electrochemical analysis demonstrates improved corrosion resistance at lower pressures in both sulfuric acid and sodium chloride electrolytes. The study concludes that reduced ambient pressure enhances bead formation, microstructure, and corrosion resistance in the laser wire-fed additive manufacturing of 4043 Al alloy [48].

Eimer et al. used wire laser arc additive manufacturing (WLAM) process to deposite aluminum zinc alloys. The WLAM system uses a gas metal arc power source to generate a melt pool and a laser beam to control the melt pool size, enabling the production of elongated melt pools and the addition of zinc with a cold wire without compromising process stability. The study investigates different process parameters and configurations, their effects on process stability, and the microstructure of the deposited material. The researchers demonstrated the achievement of high zinc concentration in the deposited material without macro-segregation [49].

Abuabiah et al. investigated geometric morphological properties, preparing an initial draft covering bead deposition modeling, monitoring and control systems, and path planning for 3D printing. The methodology included parametric modeling, experimental data analysis, and the development of monitoring and control systems. The study aimed to address the current limitations in LWAM technology and identify potential areas for improvement [50].

Sun et al. deposited single-layer and five-layer using WLAM experiments to validate transformed phases and thickness predictions. DCPM algorithm was used to simulate phase transformations in Ti-6Al-4V during cooling. The study successfully validated the accuracy of the density-based constituent phase simulation method through single-layer and five-layer deposited WLAM experiments [51].

2.4 Hybrid Additive Manufacturing

Liming et al. used three different methods using hybrid laser–TIG (LATIG) welding, laser beam welding (LBW), and gas tungsten arc (TIG) welding to weld AZ31B magnesium alloy. The welding trials were conducted using specific power sources and electrode configurations. The macrosection of the weld bead and penetration were analyzed for each welding method. Additionally, the welding stability and element distribution in the fusion zone were investigated. The study also involved microstructural analysis of the welded joints. The outcomes of this research is that the welding speed of LATIG is higher than that of TIG and is comparable to LBW. Additionally, LATIG shows double the penetration of TIG and four times that of LBW. The hybrid welding process also improves arc stability, especially at high welding speeds and low TIG currents. In terms of microstructure, the heat-affected zone is only observed in TIG welding, with coarse grain size. In the fusion zone, equiaxed grains are present, with the smallest size in LBW and the largest in TIG welding. Furthermore, the magnesium concentration in the fusion zone is lower than that of the base zone in all three welding processes [52].

Bîrdeanu et al. discussed a study on a variant of the laser-arc hybrid welding process that combines pulsed laser welding with pulsed TIG welding. The experimental work involved video data acquisition and thermal imaging to analyze the process dynamics. The study also involved metallographic assays to understand the influence of process parameters on the processing results and correlations to the process dynamics. The experimental program for characterizing the welding process variant dynamics involved several steps, including preliminary experimental work, experiments with different variants, and experiments with increased travel speed. Experiments with different process variants, such as pulsed TIG-laser, pulsed laser-TIG, and experiments without laser gas protection, to identify the recommended variant for controlling the pulsed laser welding specific penetration variation. The results revealed significant interactions between process parameters, leading to extended possibilities to influence process stability and results. The study also identified the recommended variant to attenuate the specific penetration variation of pulsed laser welding [53].

Gao et al. used a hybrid Kriging-GA model to optimize welding process parameters in hybrid fiber laser-MIG butt welding on 316L stainless steel. The process includes three main parts: Design of Experiment (DOE), Kriging model, and Genetic Algorithm (GA). The DOE involves determining the range and levels of each variable and conducting Taguchi experimental design. The Kriging model is used to approximate the relationship between process parameters and weld geometry, while the GA is utilized to optimize welding process parameters. The fitness value is defined as the predicted value obtained by the Kriging model. The outcomes of the study include the identification of dominant influencing factors on weld geometry, which were found to be power and current. The hybrid Kriging-GA model was able to optimize welding process parameters with acceptable accuracy. Additionally, the microstructure and micro-hardness of the optimized weld were found to be more beneficial for the improvement of the quality of the welded joint. These outcomes demonstrate the effectiveness of the proposed methodology in optimizing welding process parameters for hybrid fiber laser-MIG butt welding on 316L stainless steel [54].

Yan et al. compared the microstructure and mechanical properties of 304 stainless steel joints produced by TIG welding, laser welding, and laser-TIG hybrid welding. The welding process involved the use of a 5 kW CO2 laser and a conventional DCEN TIG welder. The joints were analyzed for macrostructure, microstructure, phase composition, and mechanical properties. The X-ray diffraction was used to analyse the phase composition, while microscopy and tensile tests were conducted to study the microstructure and mechanical properties of the joints. The fractured surface morphology of the specimens was analyzed using scanning electron microscopy (SEM). It was found that laser-TIG hybrid welding resulted in higher d-Fe content and a different microstructure compared to TIG and laser welding. It also observed that the absence of the heat-affected zone (HAZ) in laser-TIG hybrid welding contributed to higher tensile strength compared to TIG welding. Additionally, the study identified different fracture modes between the joints, with laser-TIG hybrid welding showing a pure-shear fracture mode [55].

William M. Steen conducted an experimental work which involved adding an electric arc to the interaction between a laser beam and a material surface. The experimental work included cutting and welding, with measurements of the bead profile taken from macro photographs of the bead cross-section. The laser used produced a beam of 10.6-μm radiation with virtually no divergence, and the power distribution within the beam approximated the fundamental Gaussian spread known as a TEM00 beam. The arc was located either on the same side of the workpiece as the laser or on the opposite side. In welding, helium shielding gas was blown coaxially with the laser beam at nozzle velocities of around 40 m/s, and in cutting, a coaxial oxygen jet of around 400 m/s was used. The experimental results showed that arc augmentation of the laser by some 2 KW of arc power in the work piece can be achieved without unduly spoiling the high quality of the cut or weld that would be made by a laser alone of similar total power. Addition of an electric arc to the interaction between a laser beam and a material surface can enhance the welding and cutting process without compromising the quality of the end product [56].

Zuo et al. utilized TIG-MIG based system for depositing 5356 aluminium alloy onto a 6061 aluminium alloy substrate. The ultimate tensile strength and microhardness increase, while ductility decreases with rising heat treatment temperature [57].

Zong et al. performed experiments on TIG-MIG hybrid welding processes, focusing on the influence of TIG current on arc stability, droplet transfer, weld formation, and temperature distribution. The study used experimental setups to analyze the welding parameters, materials, and visual inspection systems to observe the molten metal flow and temperature field on the weld pool surface. The findings suggest that TIG-MIG hybrid welding can lead to improved weld quality and reduced heat-affected zones compared to conventional MIG welding [58].

Zhang et al. used numerical analysis to study the behaviour of the molten pool and the suppression mechanism of undercut defects in TIG-MIG hybrid welding. A self-adaptive integrated model for arc welding is developed to identify factors influencing the formation of grooves, and the potential for predicting the growth rate of groove sizes based on molten pool behaviour [59].

Chapter 3
Research Gap, Motivation, Objective and Experimental Plan

3.1 Research Gap

Based on the conducted literature survey it was observed that the wire based additive manufacturing process offers various advantages such as high deposition rate, less capital cost, acceptable dimensional accuracy and others. the laser, TIG and MIG and hybrid of these power sources are typically utilised for wire based AM. The utilization of these power sources has certain advantages and limitations.
Therefore, a comparative experimental study needs to be performed while utilizing the common set of parameters and material which has not been studied.

3.2 Motivation

To identify the efficient process among wire laser, wire-TIG, wire-MIG, laser-TIG hybrid and MIG-TIG hybrid additive manufacturing process with respect to :

- Energy utilization
- Bead quality (height, width, uniformity)
- Material property (hardness)

3.3 Objective

- To investigate the hybrid processes such as Laser-TIG hybrid and MIG-TIG hybrid additive manufacturing process, and compare with WLAM, WAAM-MIG, WAAM-TIG.

- To study the process dynamics such as cooling rate during the deposition.

- To find the process influence on bead width, bead height and hardness.

- To find the most efficient process on the basis of specific energy.

3.4 Experimental Plan

For experiment, low alloy steel of 0.8 mm is used, which is the filler material which is to be melted using the arc generated by laser, TIG, MIG, laser-TIG hybrid and MIG-TIG hybrid sources and this is deposited over mild steel plate.

3.4.1 Selection of workpiece material

Mild steel is chosen as the workpiece material over which depositions are done. Mild steel is a type of carbon steel (composition by weight percentage : 0.1912% C, 0.1503% Si, 0.6702% Mn, 0.0271% P and 0.0280% S) with a low amount of carbon. Less carbon means that mild steel is typically more ductile, machinable and weldable than high carbon and other steels, however, it also means it is nearly impossible to harden and strengthen through heating and quenching. The low carbon content also means it has very little carbon and other alloying elements to block dislocations in its crystal structure, generally resulting in less tensile strength than high carbon and alloy steels. Mild steel has a lower melting point than other types of steel, so it can be welded using a lower heat setting.

3.4.2 Selection of filler material

Low alloy steel (ER70S-6) is used as a filler material for deposition. They are carbon-manganese grades, in accordance
with API or ASTM standards (e.g., AISI 4130 and AISI 8630). It is selected as a filler material because it exhibits high strength and it is highly resistant to corrosion.

3.5 Input parameters

Input parameters chosen for the experiments are power, wire feed speed and deposition speed.

3.5.1 Power

Power is the energy generated per unit time to deposit the filler material.

3.5.2 Wire feed speed

It is the speed with which wire is feed into the melt pool for deposition.

3.5.3 Deposition speed

It is the speed of deposition with which the filler metal melts and deposits over the workpiece material.

3.6 Output parameters

The output parameters chosen for the experiments are bead width, bead height, hardness, cooling rate and specific energy.

3.6.1 Bead width

It is the dimension of the bead along the width.

3.6.2 Bead height

It is the dimension of the bead along the height.

3.6.3 Hardness

Hardness is the resistance of a material to localised plastic deformation. Hardness can be assessed by a number of techniques including indentation, scratch and rebound hardness measurements.

3.6.3.1 Vickers microhardness

Vickers microhardness is a measure of a material's resistance to indentation or penetration by a Vickers indenter. The Vickers hardness test involves applying a known load to the surface of the material using a pyramidal diamond indenter with a square base and a specified angle between opposite faces (usually 136°). The indentation produced by the indenter is measured diagonally, and the Vickers hardness value is calculated based on the dimensions of the indentation and the applied force.

The Vickers hardness number (HV) is determined using the formula:

$$HV = 1.854x(F/D^2) \qquad (3.1)$$

Where,
HV : Vickers hardness number in kg/mm^2
F : Applied load in kg
D : Mean of the two diagonals in mm

3.6.4 Cooling rate

Cooling rate in welding refers to the speed at which the welded joint or the surrounding base metal cools down after the welding process is completed. It's a critical factor in determining the microstructure and mechanical properties of the weld metal and the heat-affected zone (HAZ). During welding, the base metal and the weld metal are heated to high temperatures to enable fusion and create the desired joint. After the welding arc or heat source is removed, the metal begins to cool. The rate at which this cooling occurs can significantly influence the resulting microstructure and properties of the welded joint. The cooling rate depends on several factors, including:

- Heat input: The amount of heat introduced into the base metal and the weld metal during welding, which is influenced by welding parameters such as current, voltage, travel speed, and heat source characteristics.

- Base metal composition: Different materials have varying thermal conductivities and heat capacities, affecting how quickly they dissipate heat.

- Thickness of the material: Thicker materials generally cool more slowly than thinner materials due to their higher thermal mass.

- Preheat and post-weld heat treatment: Preheating the base metal before welding and applying post-weld heat treatments can alter the cooling rate and affect the resulting microstructure and properties.

- Heat sink effect: The presence of surrounding material that acts as a heat sink can influence the cooling rate of the welded joint.

Rapid cooling can lead to the formation of hard and brittle microstructures such as martensite, which may result in increased susceptibility to cracking.

Cooling rate is determined using the formula :

$$CR = (T_m - T_o)/t \qquad (3.2)$$

Where,
CR : Cooling rate in °C/s
T_m : Melting temperature in °C (melting temperature of low alloy steel considered for the experiment is 1400 °C)
T_o : Ambient temperature in °C (melting temperature of low alloy steel considered for the experiment is 250 °C)

3.6.5 Specific energy

Specific energy is the energy required to deposit unit volume of material. The specific energy is determined by the formula :

$$SE = P/((\pi/4) x d^2 x wfs) \qquad (3.3)$$

Where,
SE : Specific energy in J/mm^3
d : Diameter of wire in mm
wfs : Wire feed speed in m/min

Chapter 4
Experimental Setup, Instruments and Softwares Used

Depositions are performed in various AM processes like Wire Laser, Wire TIG, Wire MIG, Laser-TIG hybrid and MIG-TIG hybrid

4.1 Wire Laser Additive Manufacturing (WLAM) Setup

A Fiber Laser with 4 axis is used for deposition as shown in Fig. 8 . Maximum power of the Laser is 2kW. ER70S-6 steel wire of 0.8 mm diameter was used as the wire electrode (deposition material).

Fig. 8: Wire-Laser Additive Manufacturing Setup

4.2 WAAM TIG Additive Manufacturing Setup

The experiment was carried out with a TIG (AC/DC) welding machine (make: Kemppi, model: MasterTig MLS 3003ACDC) as shown in Fig. 9 It is equipped with the standard features such as HF (high-frequency) start, the remote control using a foot pedal, and manual control to set the arc current. A straight neck water-cooled torch was used for the purpose. This type of torch is desirable for automated systems for ease of mounting on CNC (Computer Numerical Control) machines for automated welding. The utilised electrode is 2% thoriated tungsten electrode of diameter 2.4 mm. Argon gas was used as an inert gas at a constant flow rate of 10 l/min. All the experiments were conducted on the DC mode of operation, keeping the straight polarity (DCEN- Direct Current Electrode Negative). ER70S-6 steel wire of 0.8 mm diameter was used as the wire electrode (deposition material).

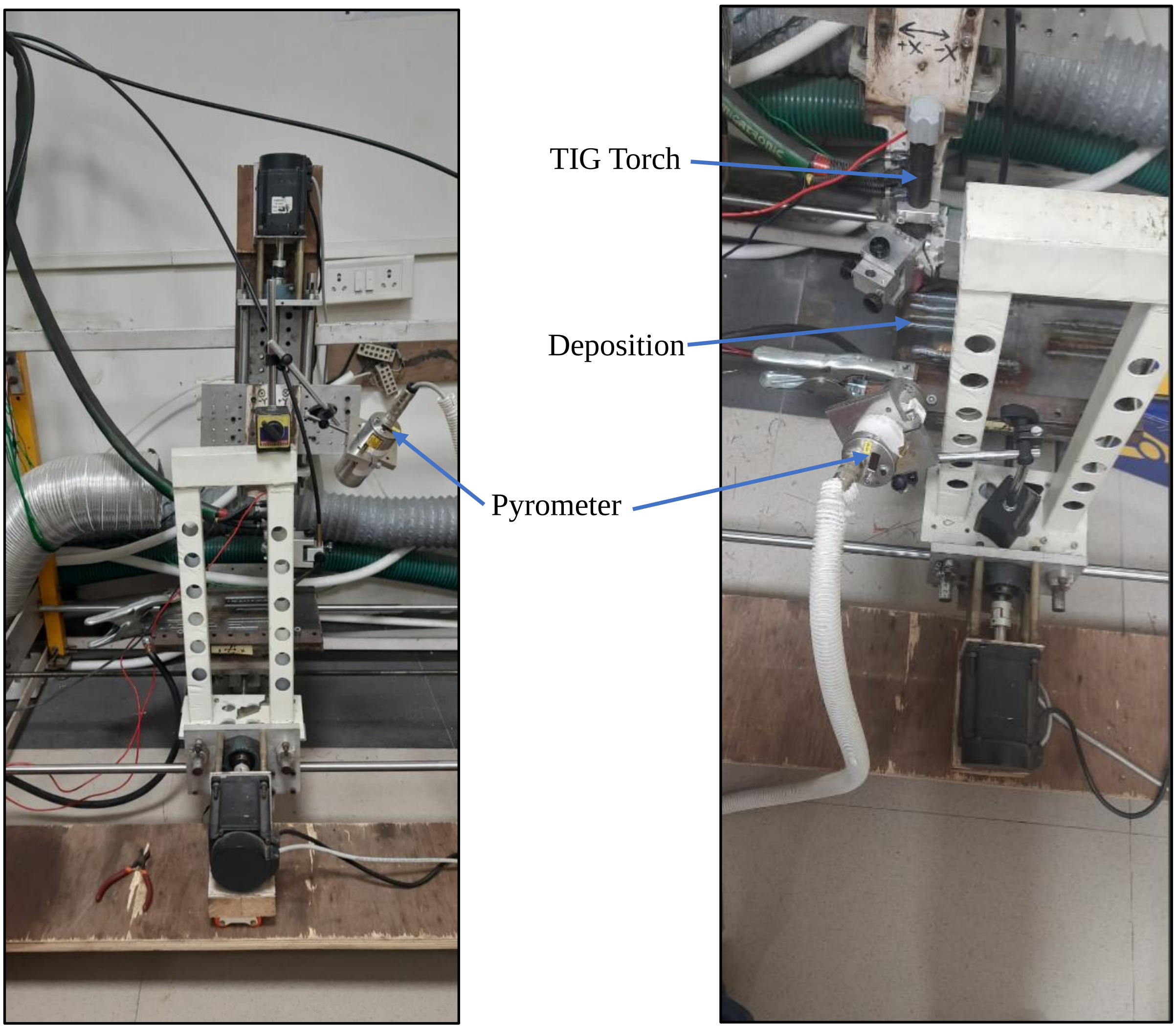

Fig. 9: Wire-TIG Additive Manufacturing Setup

4.3 WAAM MIG Additive Manufacturing Setup

MIG machine used in our case is MIGATRONIC SIGMA SELECT 400. Mig torch comprises handle, trigger, nozzle and contact tip, it enables a continuous feed of the consumable electrode wire. The wire serves as both electrode and filler material, melts at the arc's heat, forming a molten pool that solidifies to create a required weld part. Shielding gas is also supplied from the nozzle itself and helps in forming a smooth deposition. The MIG torch is fixed using a burette stand with is connected with the linear stage.

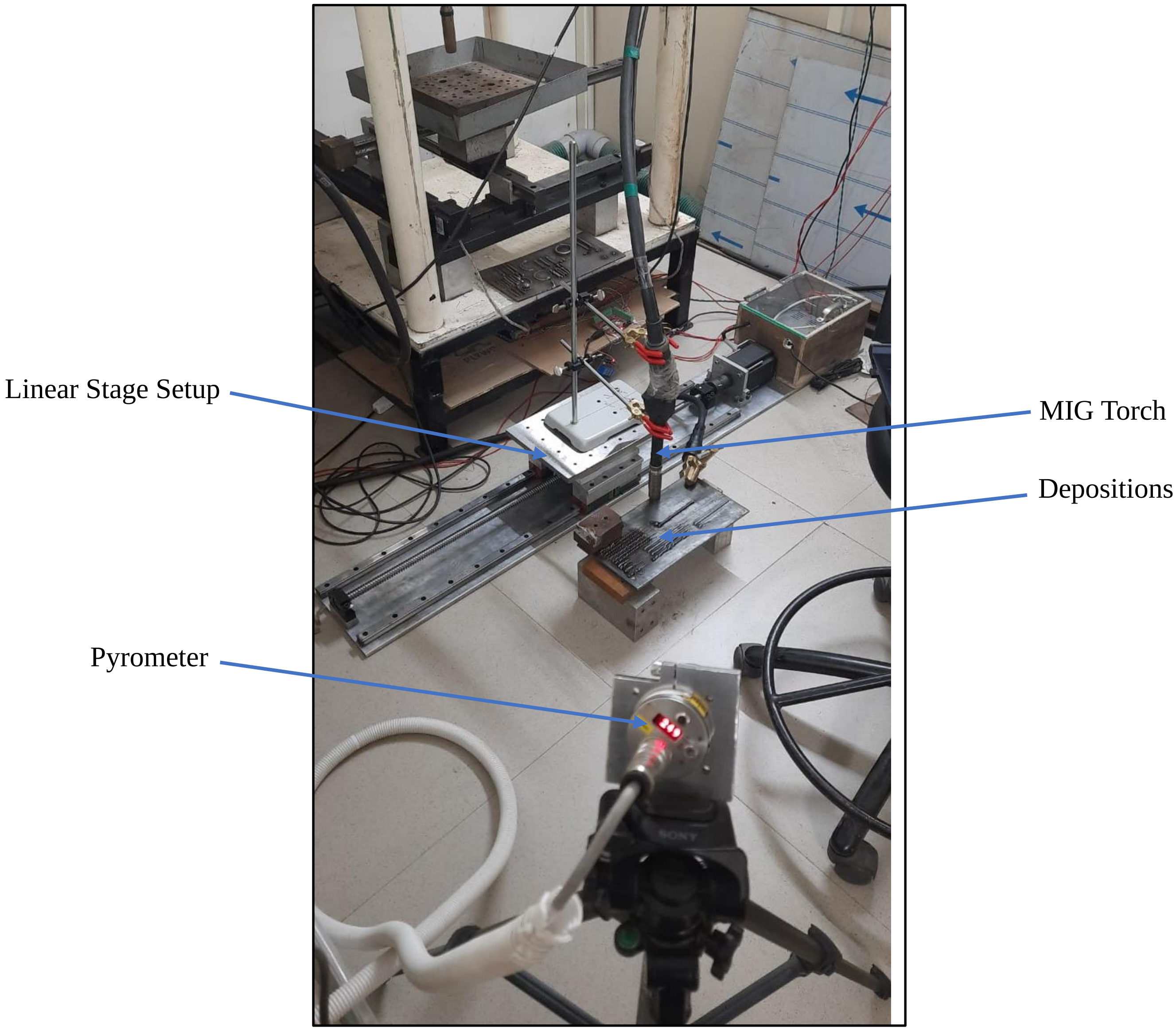

Fig. 10: Wire MIG Additive Manufacturing Setup

4.4 Laser-TIG Hybrid Additive Manufacturing setup

A Fiber Laser with 4 axis is used for deposition as shown in Fig. 11. Maximum power of the Laser is 2kW. A straight neck air-cooled TIG torch was used for the purpose. The torch was mounted in the wire laser welding machine using the two fingered clamps with rubber gripper. The angle between laser and TIG torch is 65˚. ER70S-6 steel wire of 0.8 mm diameter was used as the wire electrode (deposition material).

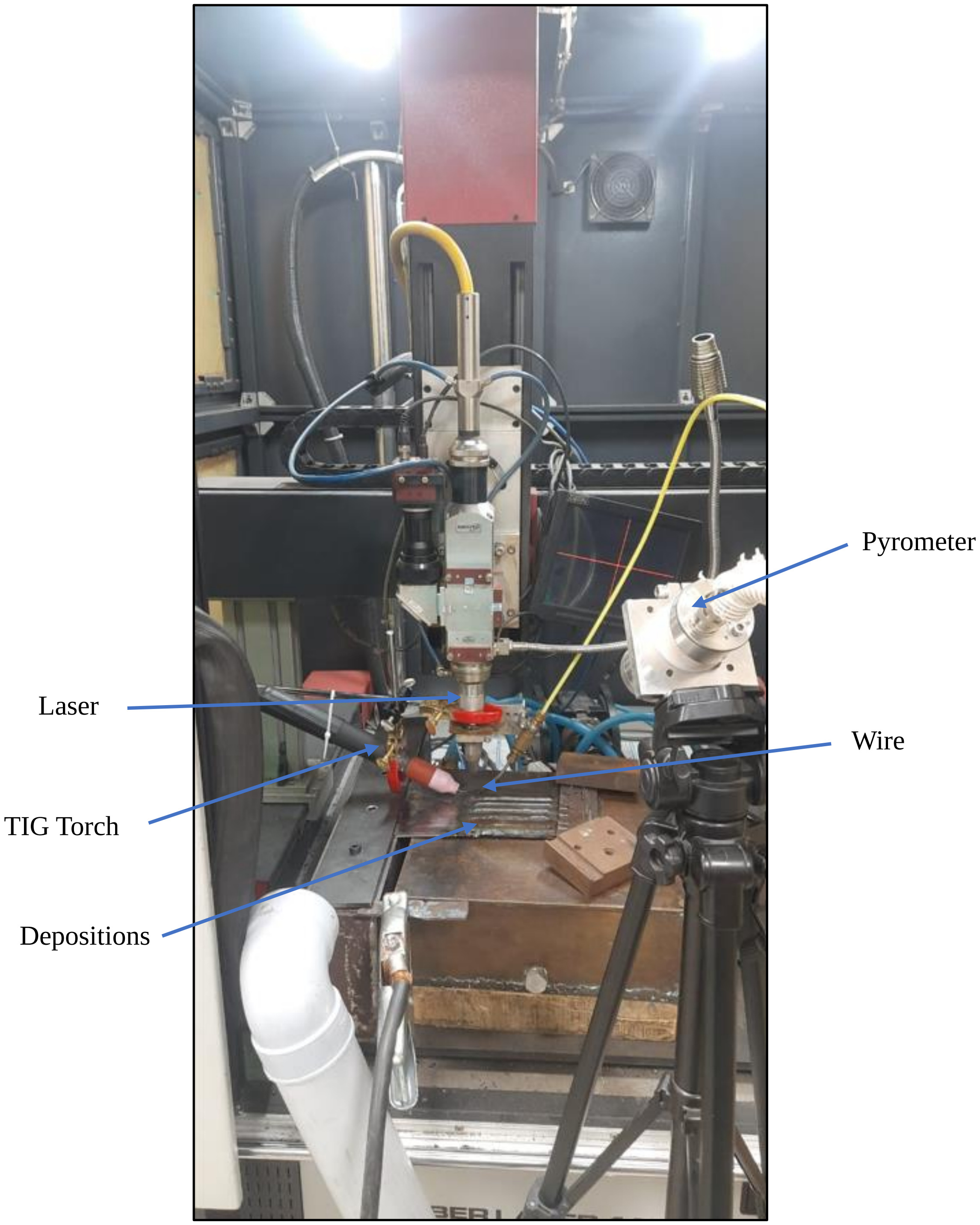

Fig. 11: Laser-TIG Hybrid Additive Manufacturing Setup

4.5 MIG-TIG Hybrid Additive Manufacturing setup

The MIG torch which was used in MIG deposition is used here. The same air cooled TIG torch used in Laser-TIG hybrid deposition is used here. The TIG torch was mounted in MIG welding system using two fingered clamps with rubber gripper. The angle between the MIG torch and TIG torch is 25°.

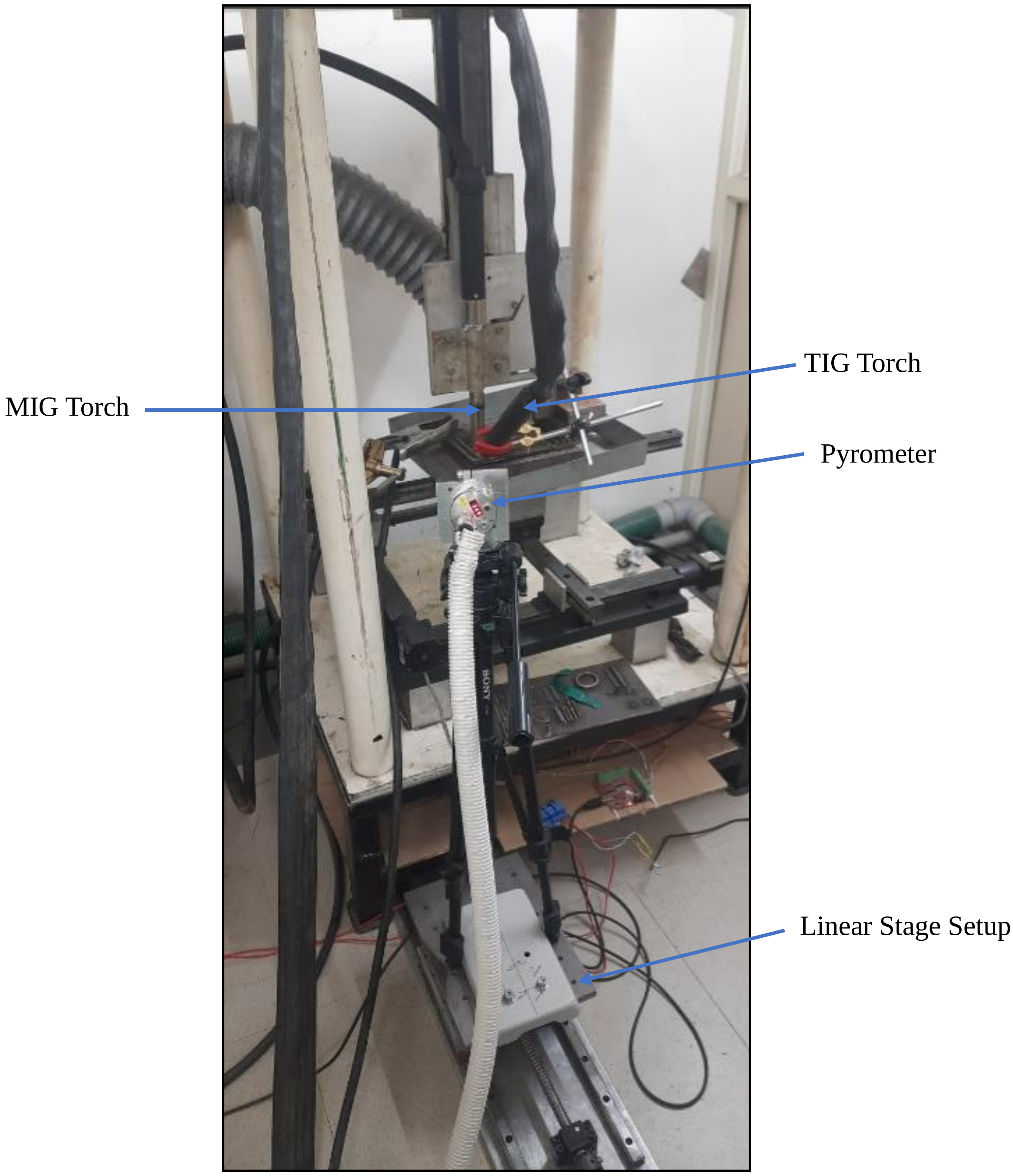

Fig. 12: MIG-TIG Hybrid Additive Manufacturing Setup

4.6 Linear Stage Setup

The linear stage setup is used for MIG deposition and MIG- TIG hybrid deposition. The linear stage setup consists of railings, lead screw, bearings, linear bearings, first base plate of aluminium and second base plate of mild steel. A I section of asbestos is used as an insulator.

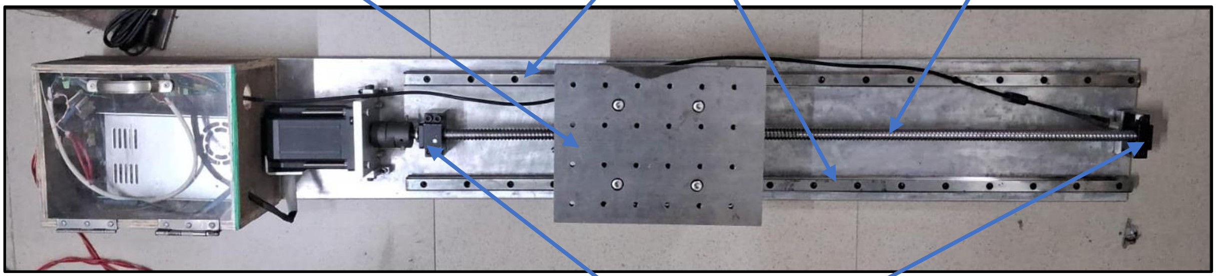

Fig. 13: Top view of Linear Stage

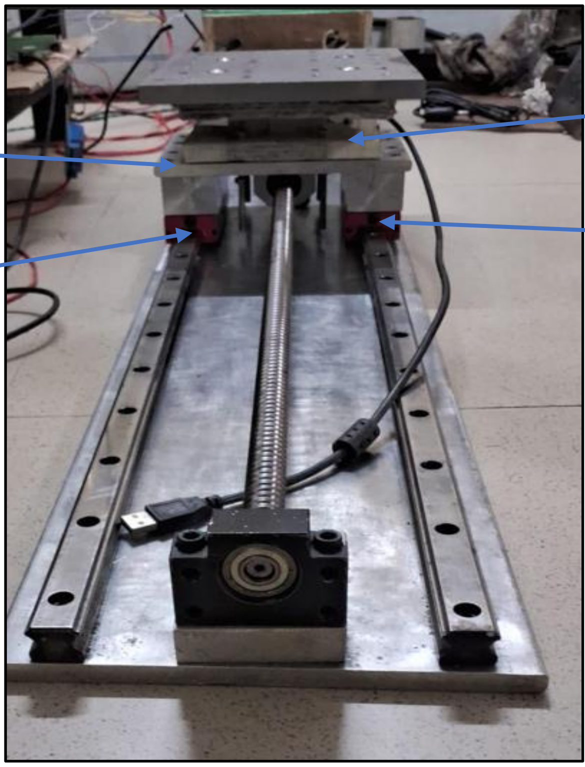

Fig. 14: Side view of Linear Stage

4.7 Pyrometer

The pyrometer used for the measurement of temperature was the ratio pyrometer model IGAR 6. A detailed view of the pyrometer is shown in the figure below:

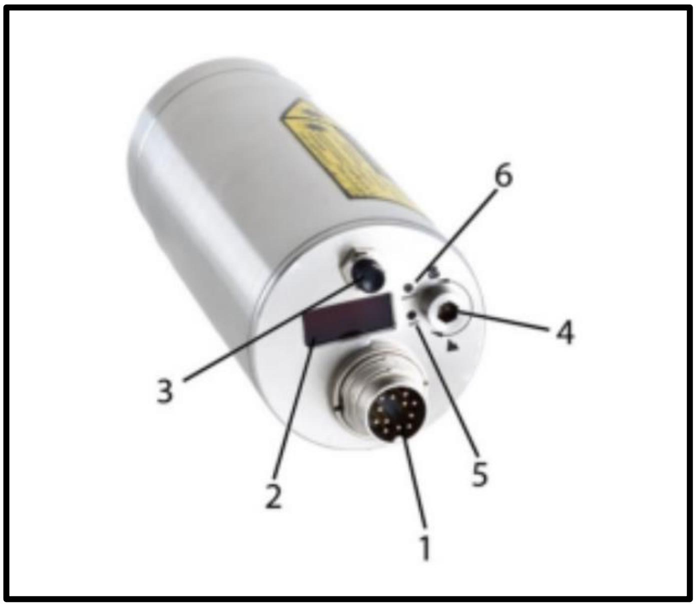

Fig. 15: Pyrometer

1. 12-Pin Connector
2. Digital Display
3. Sighting Option
4. Focus Adjustment Set Screw
5. LED Distance Indicator Light
6. LED Operating Mode Indicator Light

4.8 Laser Displacement Sensor

M/s Micro-Epsilon make smart laser triangulation displacement sensor (LDS), model: optoNCDT 1420 with active surface compensation property is used to scan the objects. It provides displacement, distance and position measurement with a unique combination of speed, size, performance and application versatility with a high measurement accuracy. LDS uses a laser diode and works on the basis of the Time-of-Flight (ToF) principle to measure the distance between its sensor and an object. LDS internally determines the distance based on the time elapsed between emitting and receiving the laser beam from the surface. This sensor is used to measure the bead height and bead width of the deposited beads.

Fig. 16: Laser Displacement Sensor

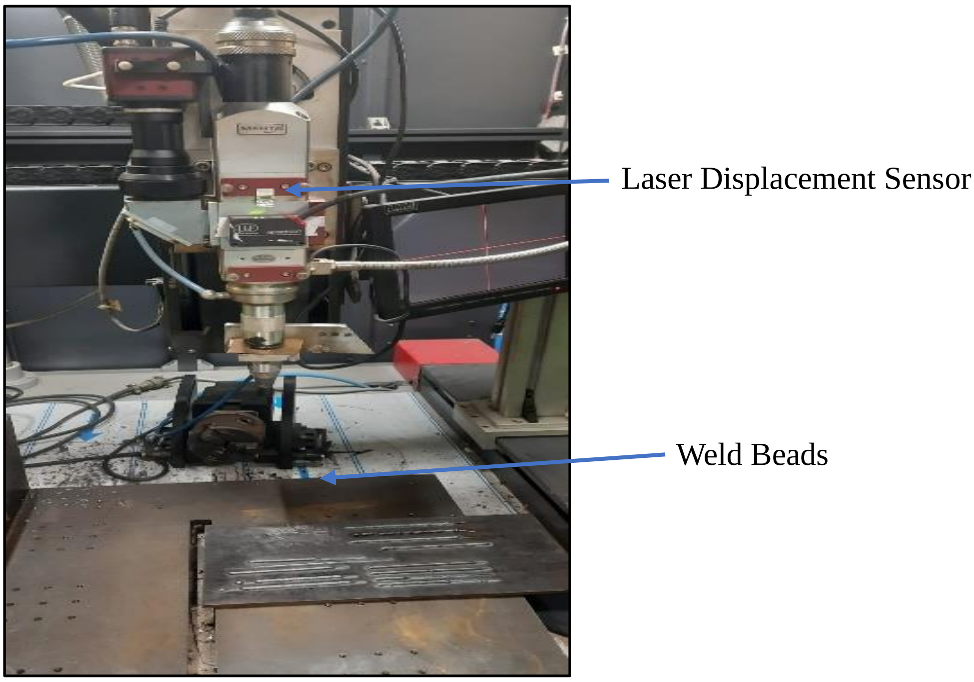

Fig. 17: Setup for measuring bead width and height

4.9 Abrasive Cutting Machine

Abrasive cutting machine make METNATION TECHNOLOGIES is used to cut the weld beads.

Fig. 18: Abrasive Cutting Machine

4.10 Polishing Machine

The cut samples were polished using a polishing machine of make METCO BAINPOL.

Fig. 19: Polishing Machine

4.11 Hardness Testing Machine

Vickers micro hardness testing machine of make METCO Economet VH-1 MDX is used to measure the hardness of the polished samples. The Vickers micro hardness testing machine consists of a diamond indenter, which falls over the sample and it stays over the object for a particular time and then it moves away from the sample. This time interval between the loading and unloading of the indenter is known as the delay time. After that the length of the diagonals are measured and the hardness value is given by this machine. This hardness testing machine has load range from 0.1 kg to 0.5 kg

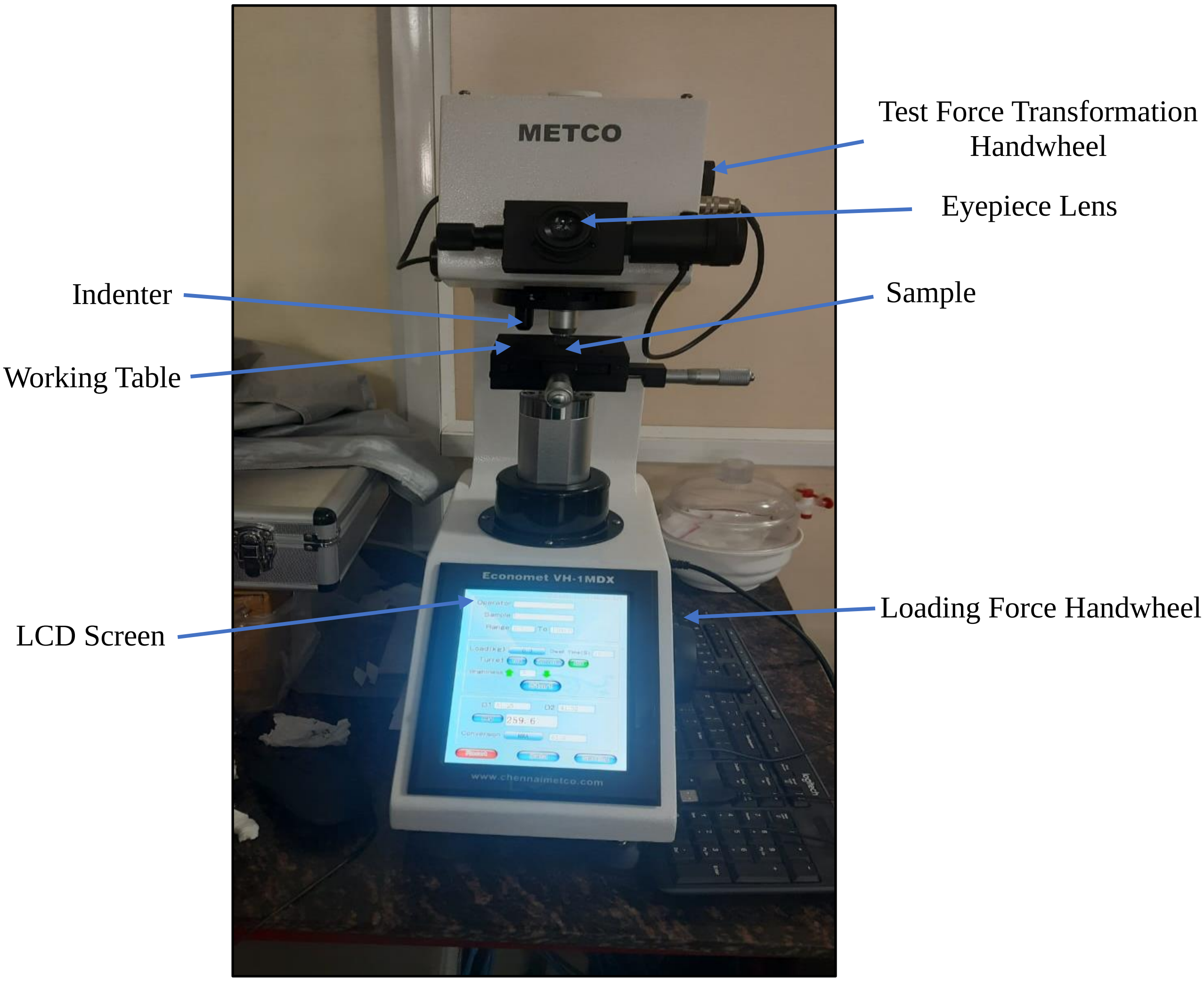

Fig. 20: Vickers Microhardness Testing Machine

4.12 Infrawin

This is a software to collect data from pyrometer which gives the data in the form of temperature and time.

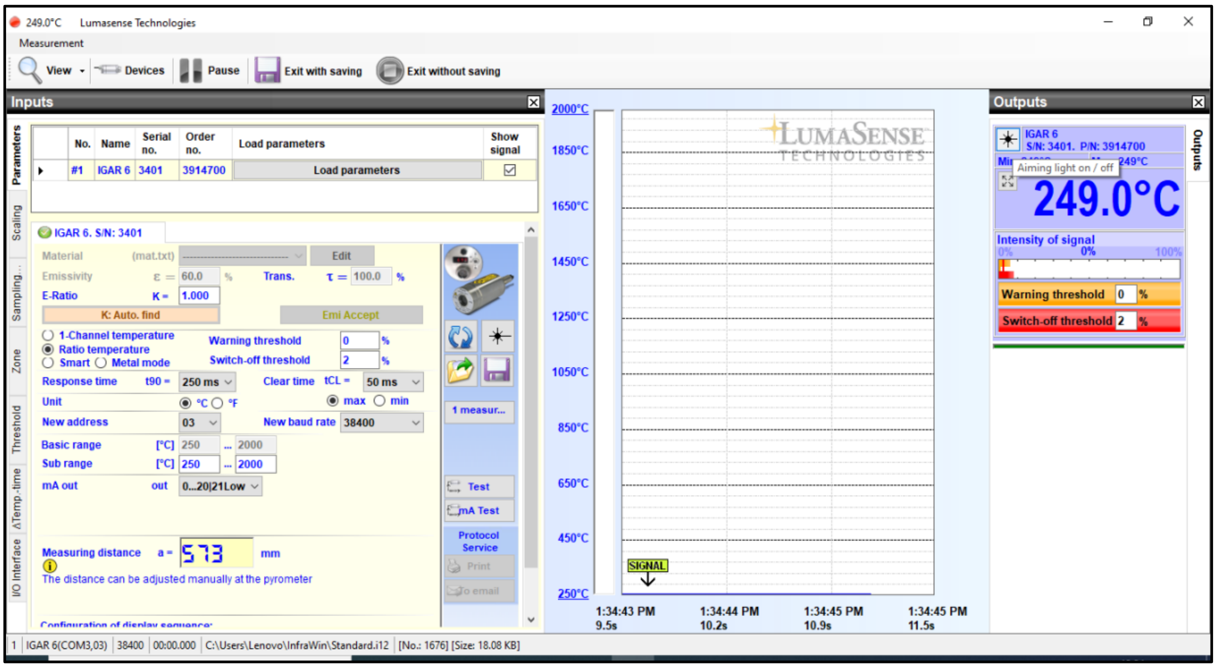

Fig. 21: Infrawin software

4.13 Mach 3 :

Mach3 is a full-featured CNC controller that uses G and M codes to transform a computer into a machine controller.

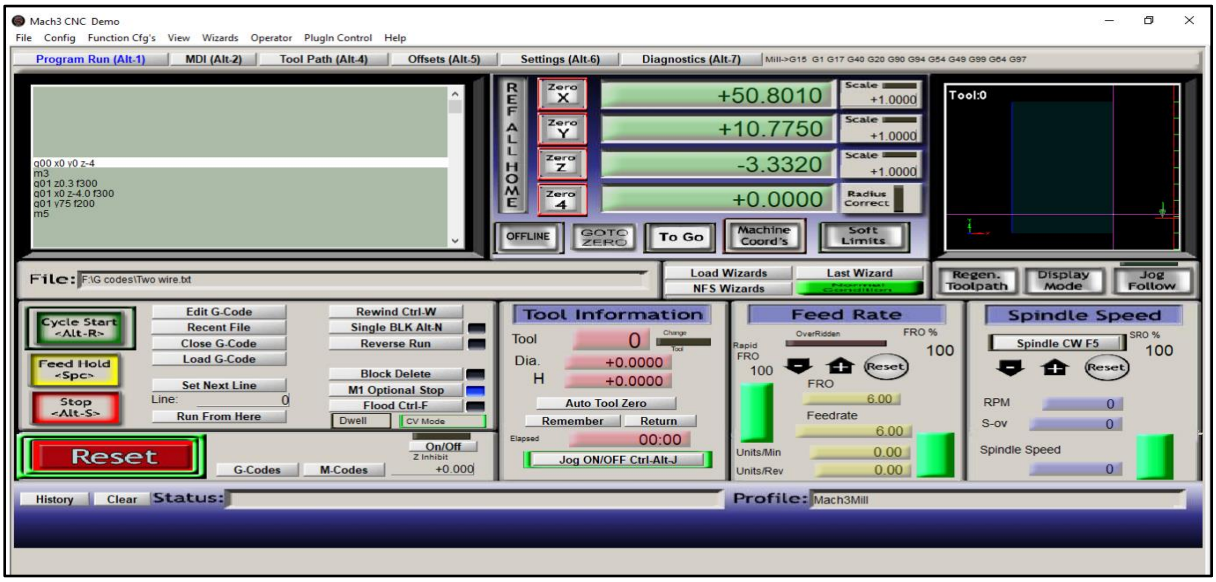

Fig. 22: Mach 3 software

Chapter 5
Results and Discussion for WLAM

In WLAM the input parameters are wire feed speed, deposition speed and power. Wire feed speed and deposition speed are kept constant. The power is varied for doing the depositions. Three linear depositions of length 100 mm are being done.

5.1 Input parameters

Table 2: Input parameters used in WLAM depositions

Power (W)	1200	1300	1400
Wire Feed Speed (m/min)		2	
Deposition Speed (mm/min)		100	

5.2 WLAM depositions

Three linear single layer depositions are done using laser as shown in the figures below. Before each deposition preheating is done to remove the oxides.

Fig. 23: WLAM deposition for 1200 W power

Fig. 24: WLAM deposition for 1300 W power

Fig. 25: WLAM deposition for 1400 W power

5.3 Temperature recording for each deposition and measurement of cooling rate

Temperature is recorded during the deposition which is obtained in the form of temperature and time. Cooling rate is calculated using the eq.3.2.

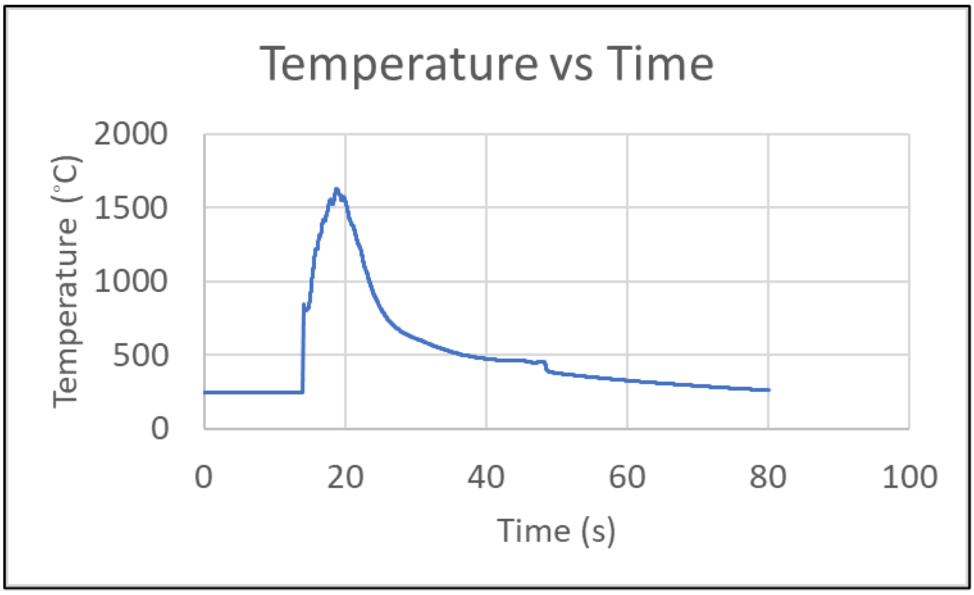

Fig. 26: Temperature vs time graph in WLAM for 1200 W power

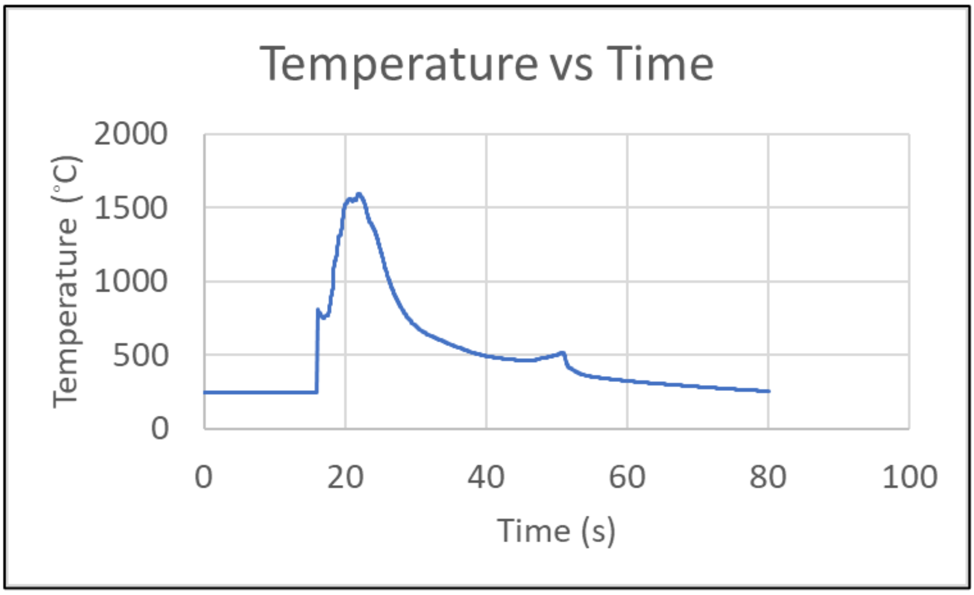

Fig. 27: Temperature vs time graph in WLAM for 1300 W power

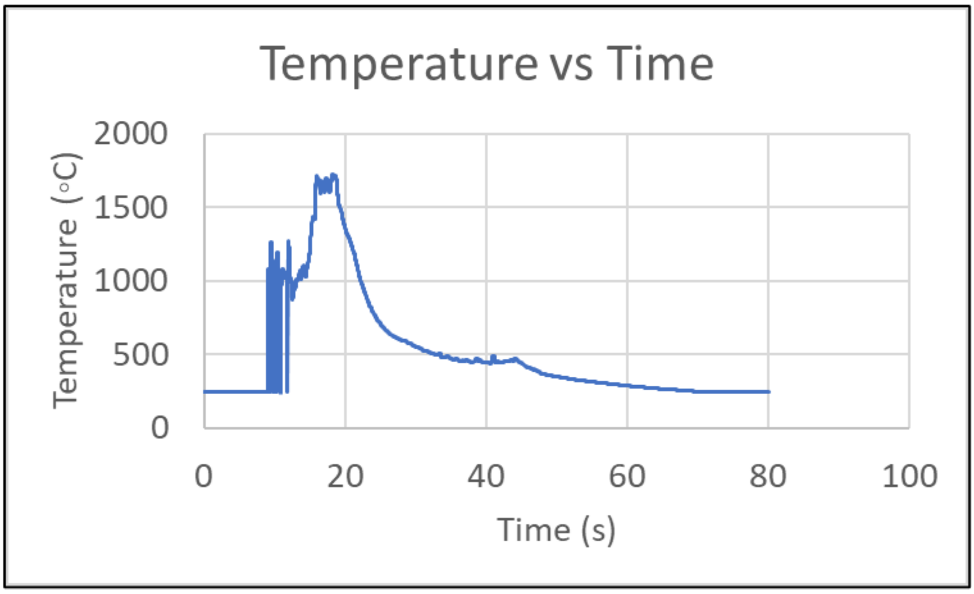

Fig. 28: Temperature vs time graph in WLAM for 1400 W power

From the temperature vs time graph cooling rate is calculated which is shown in the table below.

Table 3: Cooling rate calculated for each deposited bead using WLAM process

Power (W)	Cooling Rate (°C/s)
1200	18.06
1300	19.7
1400	23.11

A graph is plotted between cooling rate vs power is plotted.

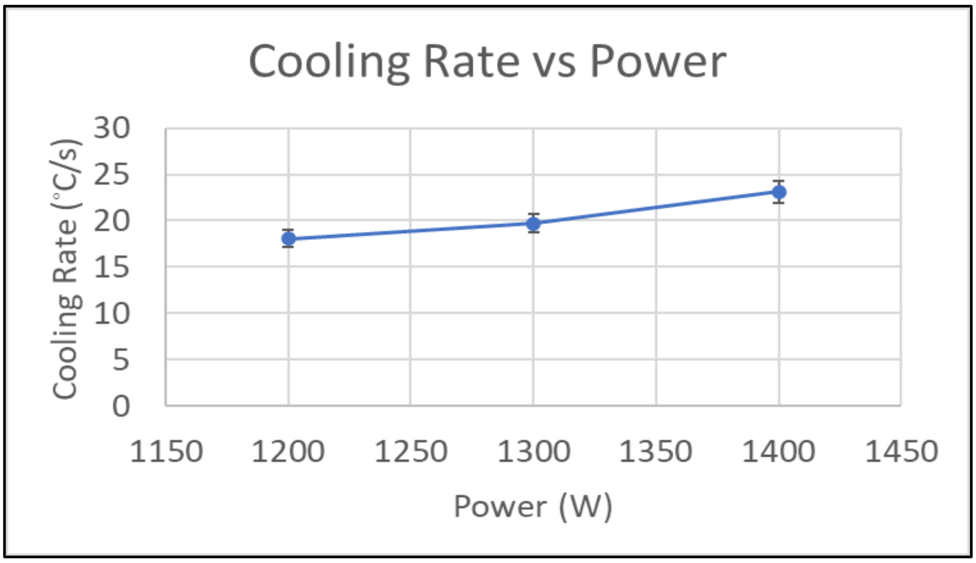

Fig. 29: Cooling rate vs power for WLAM depositions

5.4 Specific energy

Specific energy is calculated as per eq.3.3 and a graph is being plotted between specific energy vs power.

Table 4: Specific energy calculated for each power level of the WLAM deposition

Power (W)	Specific Energy (J/mm^3)
1200	71.61
1300	77.58
1400	83.55

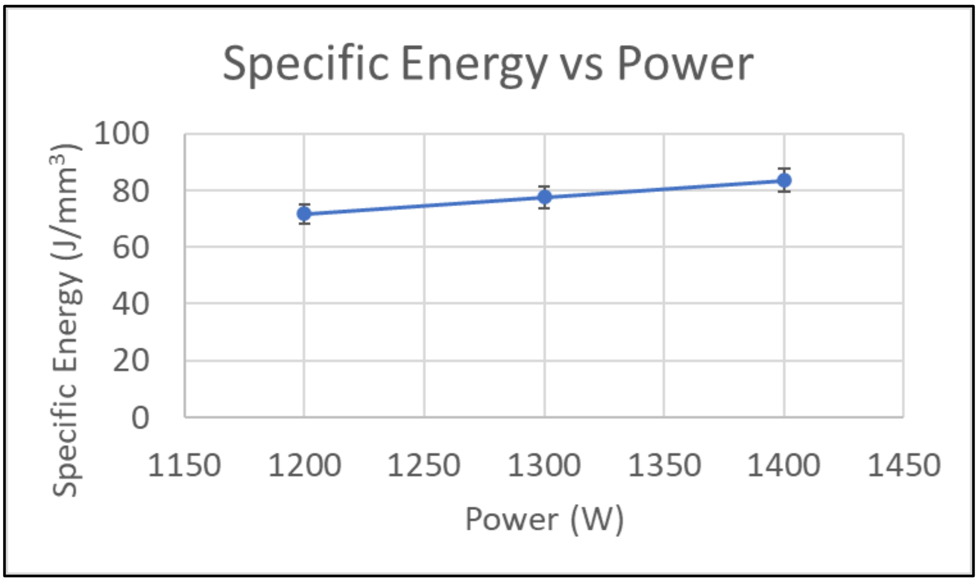

Fig. 30: Specific energy vs power for WLAM depositions

5.5 Output parameters

The output parameters are bead width, bead height and hardness which are measured after the three linear depositions the bead height, bead width and hardness are measured.

5.5.1 Bead width and bead height measurement

The bead width and bead height are measured using LDS. The width and height are measured from 40 mm from start, 50 mm from start and 60 mm from start. Then average of the values are taken and noted down.

Table 5: Bead width and bead height of deposited WLAM beads

Power (W)	Bead Width (mm)				Bead Height (mm)			
	40 mm from start	50 mm from start	60 mm from start	Mean	40 mm from start	50 mm from start	60 mm from start	Mean
1200	2.62	2.37	3.72	2.90	3.50	3.80	3.22	3.50
1300	5.82	3.81	3.04	4.22	2.94	3.79	3.38	3.37
1400	3.33	3.11	6.38	4.27	2.95	3.62	3.24	3.27

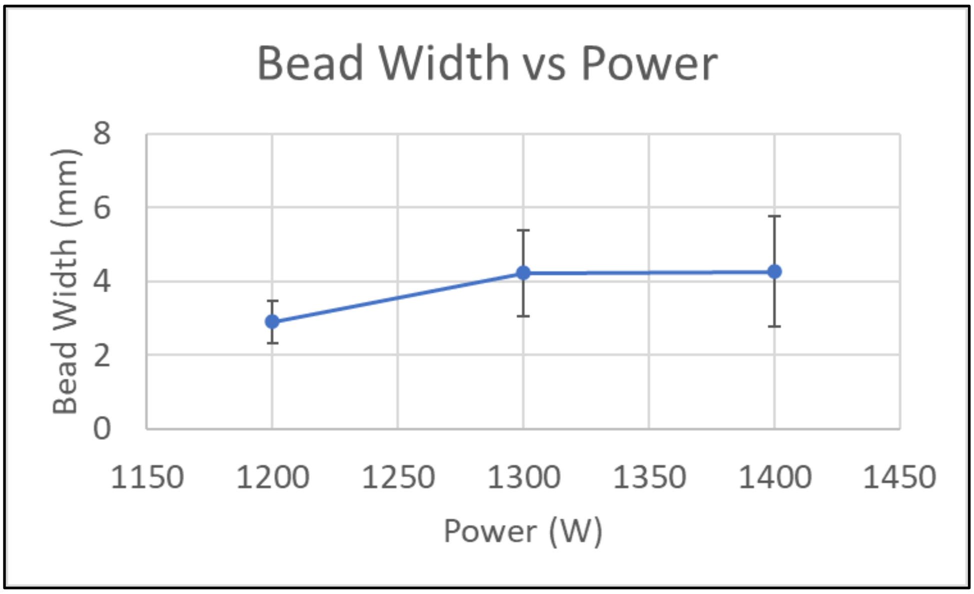

Fig. 31: Bead width vs power for WLAM depositions

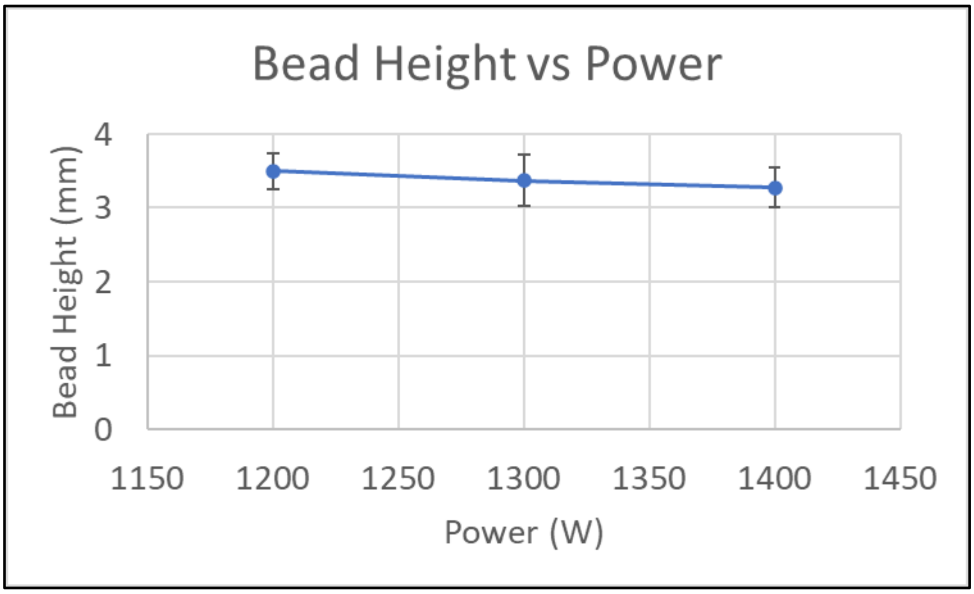

Fig. 32: Bead height vs power for WLAM depositions

5.5.2 Hardness measurement

The samples are cut using a water jet abrasive cutter along the cross section which are polished using sand paper of grit size 80 and 1000. Polishing is done upto such a level so that the samples are free from irregularities. After polishing the samples, the hardness of the samples is measured using Vickers hardness testing machine. The hardness is measured at three different positions and mean value of the readings are noted. Load of 0.3 kg is used at a dwell time of 10 s. Hardness is calculated using the eq.3.1.

Fig. 33: Cut cross of the polished WLAM weld bead, (a) 1200 W, (b) 1300 W, (c) 1400 W

Table 6 : Hardness of deposited beads in WLAM process

Power (W)	Hardness
1200	245.4
1300	257
1400	305.6

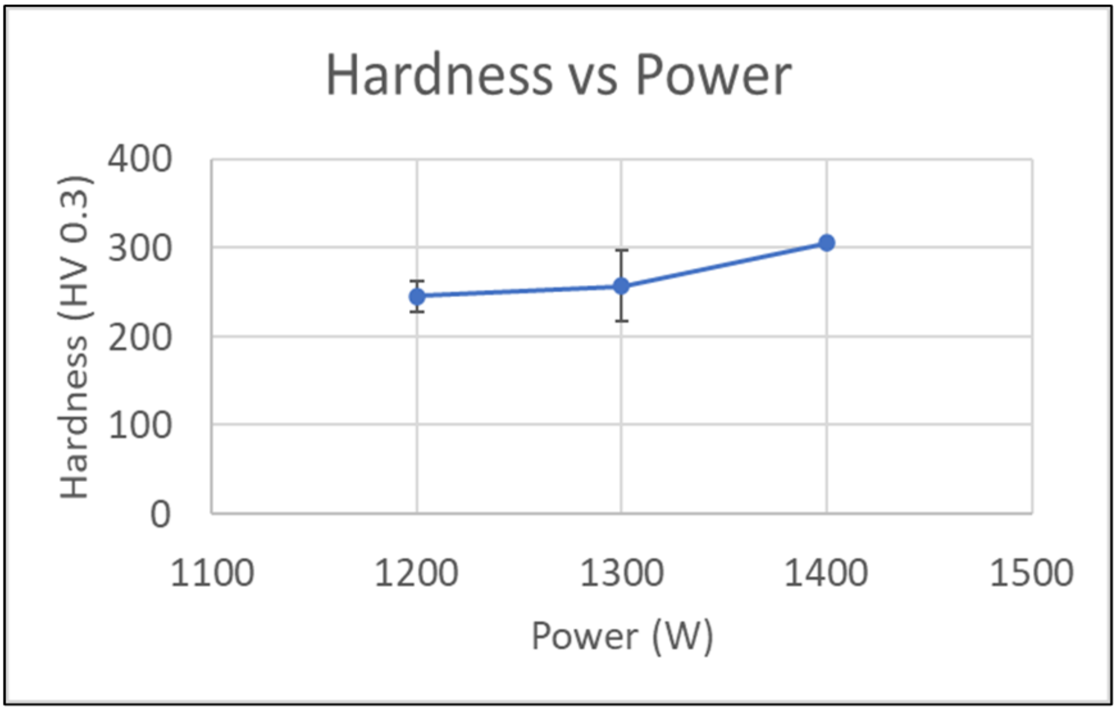

Fig. 34: Hardness vs power for WLAM depositions

Chapter 6
Results and Discussion for WAAM-TIG

In WAAM-TIG the input parameters are wire feed speed, deposition speed and power. Wire feed speed and deposition speed are kept constant. The power is varied for doing the depositions. Three linear depositions of length 100 mm are being done.

6.1 Input parameters

Table 7: Input parameters used in WAAM-TIG depositions

Power (W)	1320	1440	1560
Wire Feed Speed (m/min)	2		
Deposition Speed (mm/min)	100		

6.2 WAAM-TIG depositions

Three linear single layer depositions are done using TIG as shown in the figures below. Before each deposition preheating is done to remove the oxides.

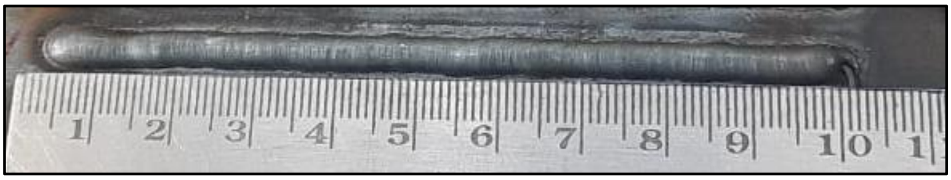

Fig. 35: WAAM-TIG deposition for 1320 W power

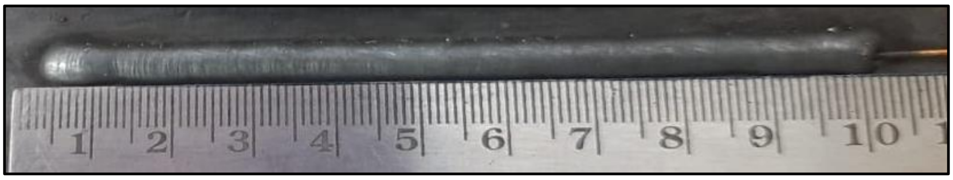

Fig. 36: WAAM-TIG deposition for 1440 W power

Fig. 37: WAAM-TIG deposition for 1560 W power

6.3 Temperature recording for each deposition and measurement of cooling rate

Temperature is recorded during the deposition which is obtained in the form of temperature and time. Cooling rate is calculated using the eq.3.2.

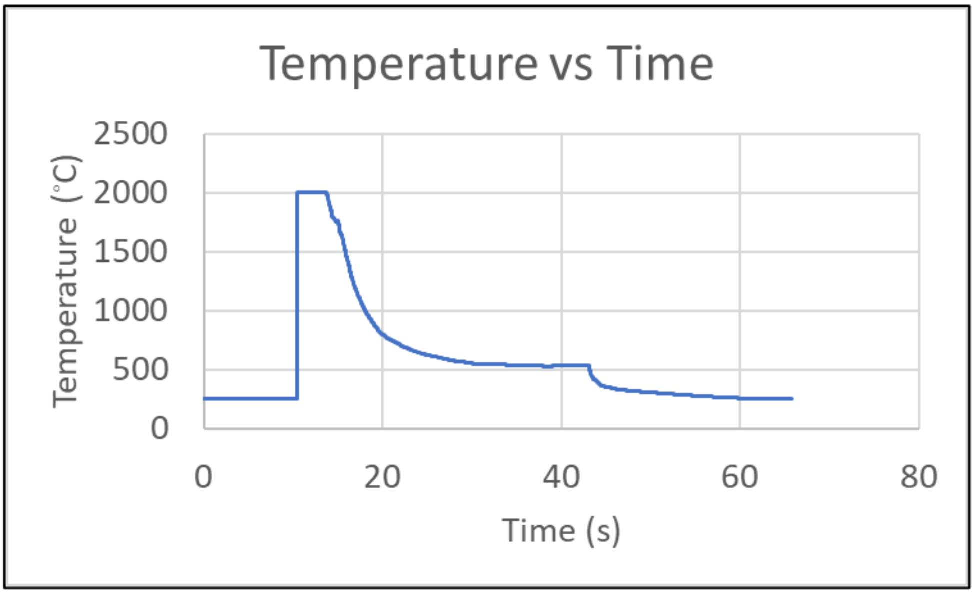

Fig. 38: Temperature vs time graph in WAAM-TIG for 1320 W power

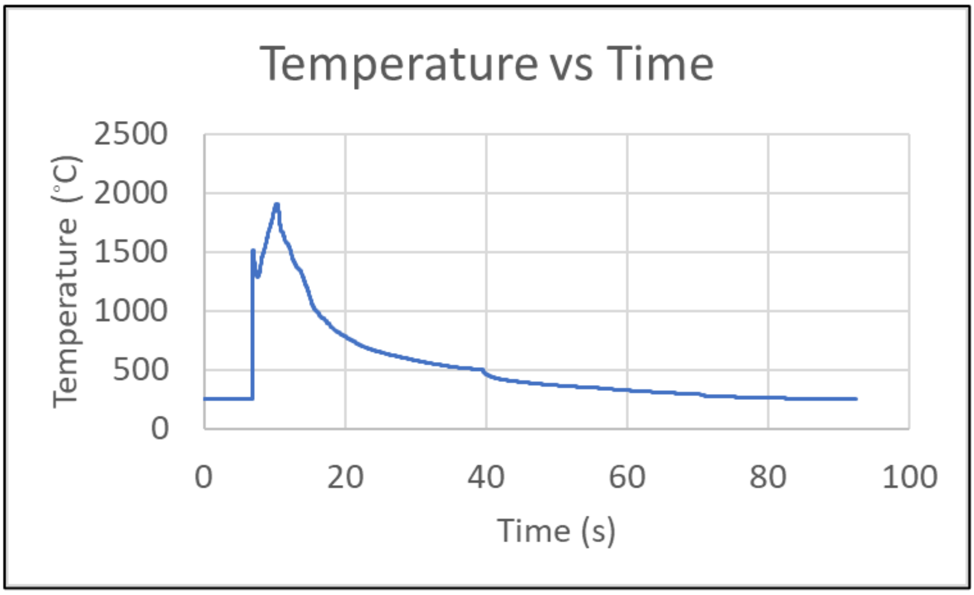

Fig. 39: Temperature vs time graph in WAAM-TIG for 1440 W power

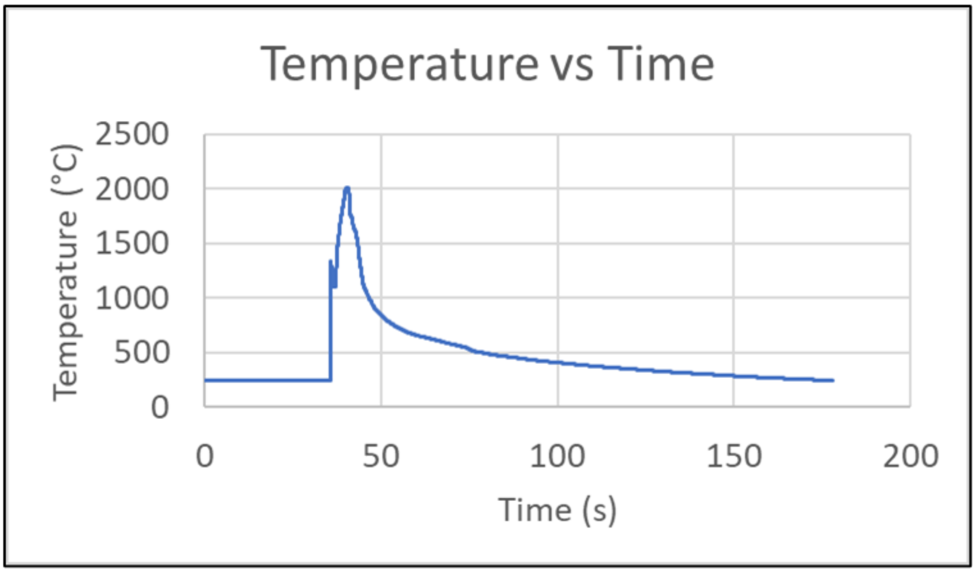

Fig. 40: Temperature vs time graph in WAAM-TIG for 1560 W power

From the temperature vs time graph cooling rate is calculated which is shown in the table below.

Table 8: Cooling rate calculated for each deposited bead using WAAM-TIG process

Power (W)	Cooling Rate (°C/s)
1320	27.15
1440	16.42
1560	9.55

A graph is plotted between cooling rate vs power is plotted.

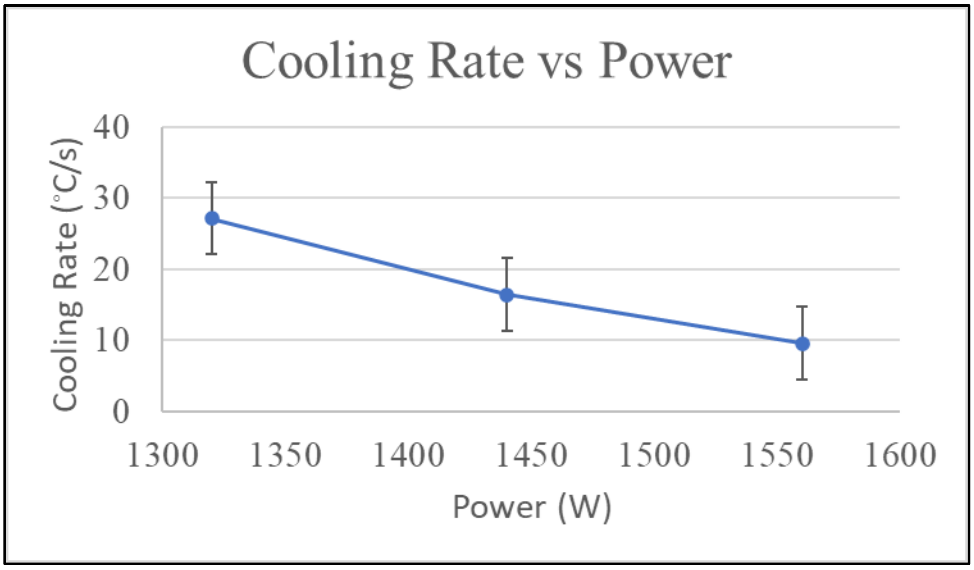

Fig. 41: Cooling rate vs power for WAAM-TIG depositions

6.4 Specific energy

Specific energy is calculated as per eq.3.3 and a graph is being plotted between specific energy vs power.

Table 9: Specific energy calculated for each power level of the WAAM-TIG bead

Power (W)	Specific Energy (J/mm^3)
1320	78.78
1440	85.94
1560	93.10

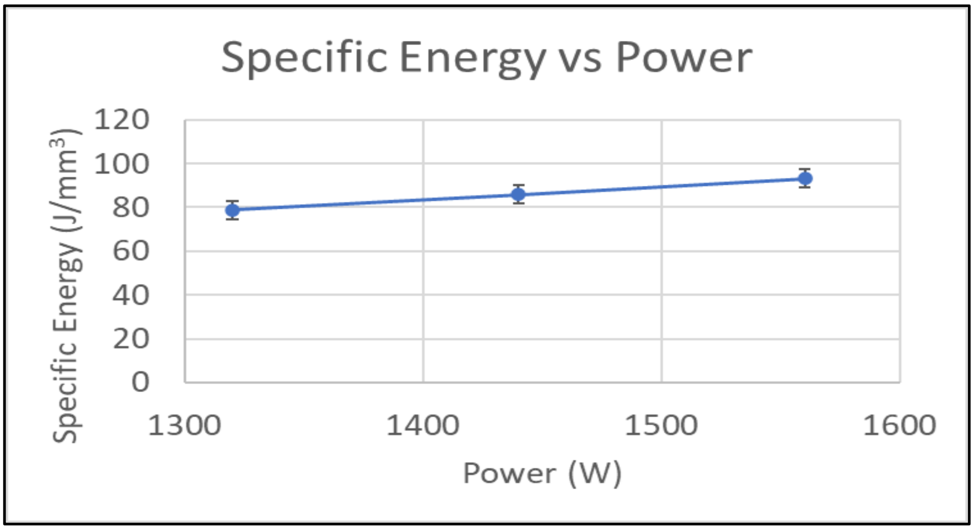

Fig. 42: Specific energy vs power for WAAM-TIG depositions

6.5 Output parameters

The output parameters are bead width, bead height and hardness which are measured after the three linear depositions the bead height, bead width and hardness are measured.

6.5.1 Bead width and bead height measurement

The bead width and bead height are measured using LDS. The width and height are measured from 40 mm from start, 50 mm from start and 60 mm from start. Then average of the values are taken and noted down.

Table 10: Bead width and bead height of deposited beads using WAAM-TIG Process

Power (W)	Bead Width (mm)				Bead Height (mm)			
	40 mm from start	50 mm from start	60 mm from start	Mean	40 mm from start	50 mm from start	60 mm from start	Mean
1320	3.37	2.49	3.96	3.27	2.05	3.24	2.38	2.55
1440	4.9	3.79	3.15	3.94	2.38	2.09	2.85	2.44
1560	5.1	6.74	4.74	5.52	2.15	2.19	2.36	2.23

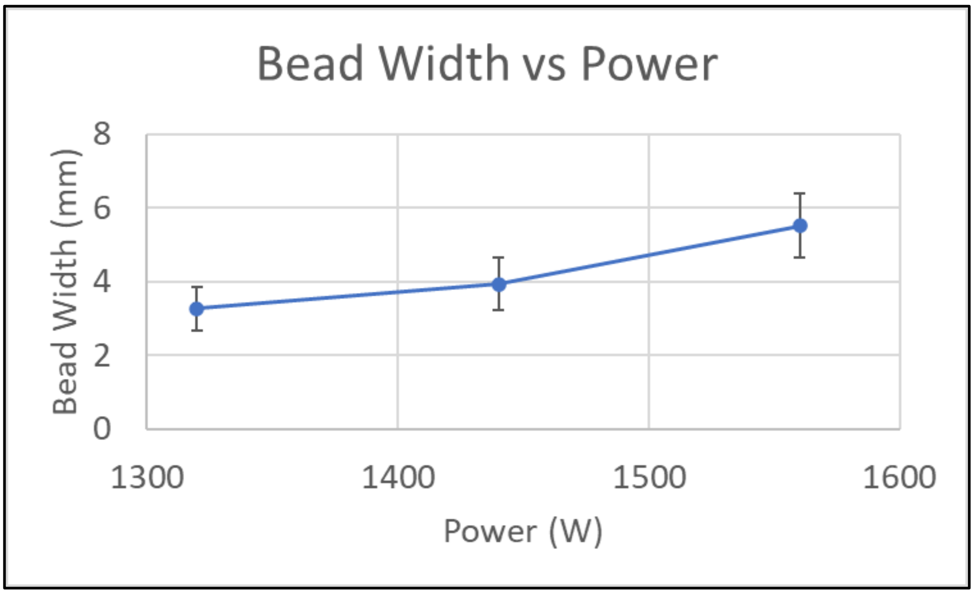

Fig. 43: Bead width vs power for WAAM-TIG depositions

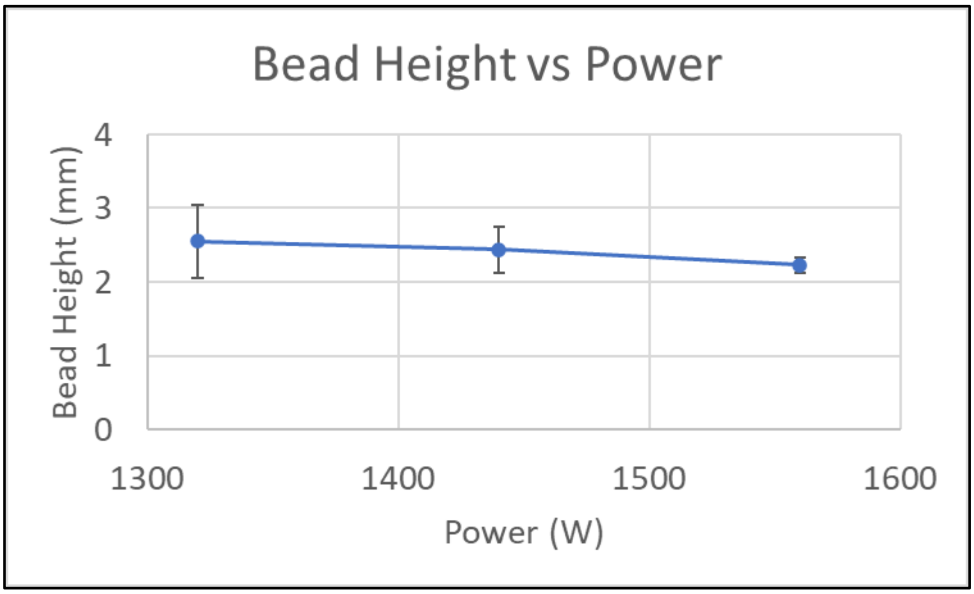

Fig. 44: Bead height vs power for WAAM-TIG depositions

6.5.2 Hardness measurement

The samples are cut using a water jet abrasive cutter along the cross section, which are polished using sand paper of grit size 80 and 1000. Polishing is done upto such a level so that the samples are free from irregularities. After polishing the samples, the hardness of the samples is measured using Vickers hardness testing machine. The hardness is measured at three different positions and mean value of the readings are noted. Load of 0.3 kg is used at a dwell time of 10 s. Hardness is measured using the eq. 3.1.

Fig. 45: Cut cross of the polished WAAM -TIG weld bead, (a) 1320 W, (b) 1440 W, (c) 1560 W

Table 11: Hardness of deposited beads in WAAM-TIG process

Power (W)	Hardness
1320	284.5
1440	270.9
1560	268.96

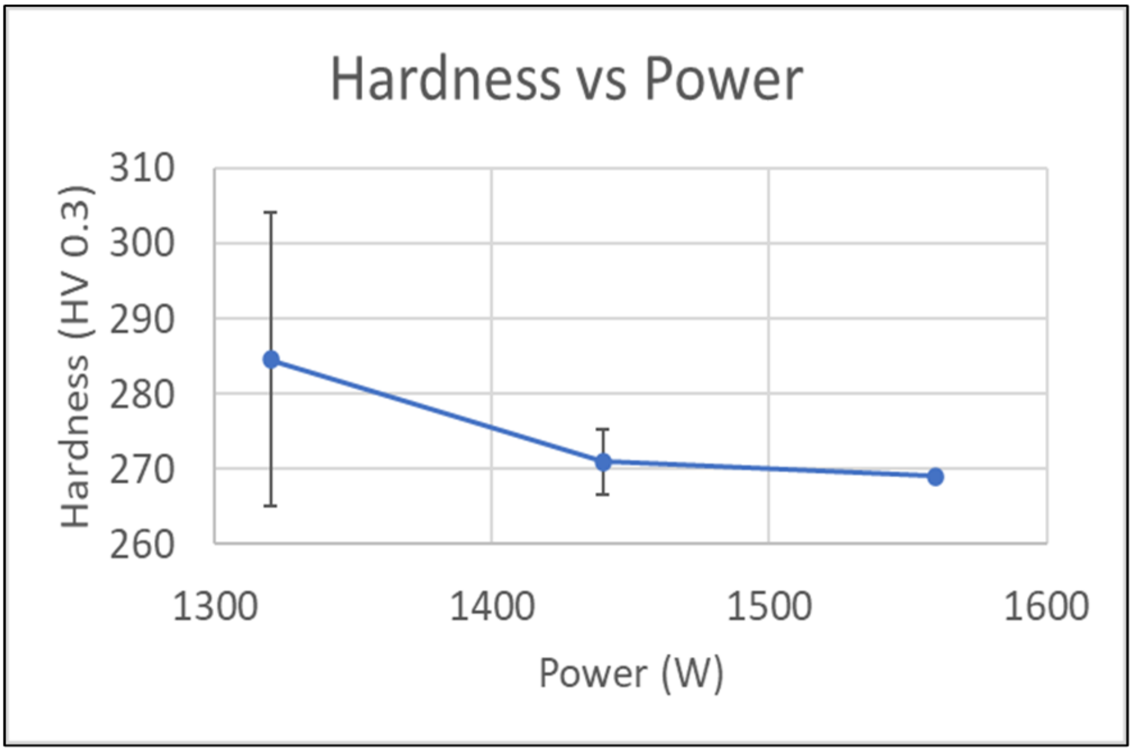

Fig. 46: Hardness vs power for WAAM-TIG depositions

Chapter 7
Results and Discussion for WAAM-MIG

In WAAM-MIG the input parameters are wire feed speed, deposition speed and power. Wire feed speed and deposition speed are kept constant. The power is varied for doing the depositions. Three linear depositions of length 100 mm are being done.

7.1 Input parameters

Table 12: Input parameters used in WAAM-MIG depositions

Power (W)	680	738	779
Wire Feed Speed (m/min)		2	
Deposition Speed (mm/min)		100	

7.2 WAAM-MIG depositions

Three linear single layer depositions are done using MIG as shown in the figures below.

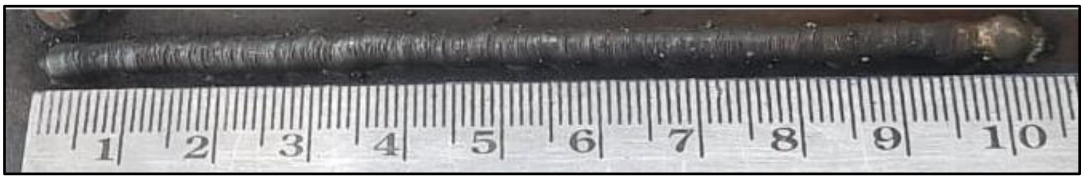

Fig. 47: WAAM-MIG deposition for 680 W power

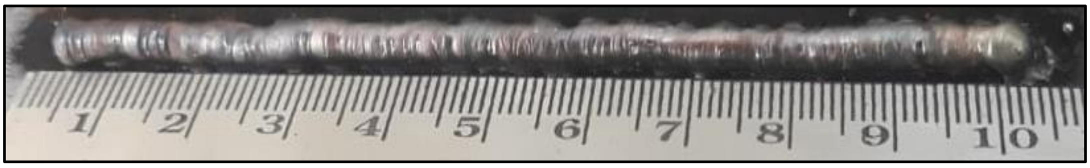

Fig. 48: WAAM-MIG deposition for 738 W power

Fig. 49: WAAM-MIG deposition for 779 W power

7.3 Temperature recording for each deposition and measurement of cooling rate

Temperature is recorded during the deposition which is obtained in the form of temperature and time. Cooling rate is calculated using the eq.3.2.

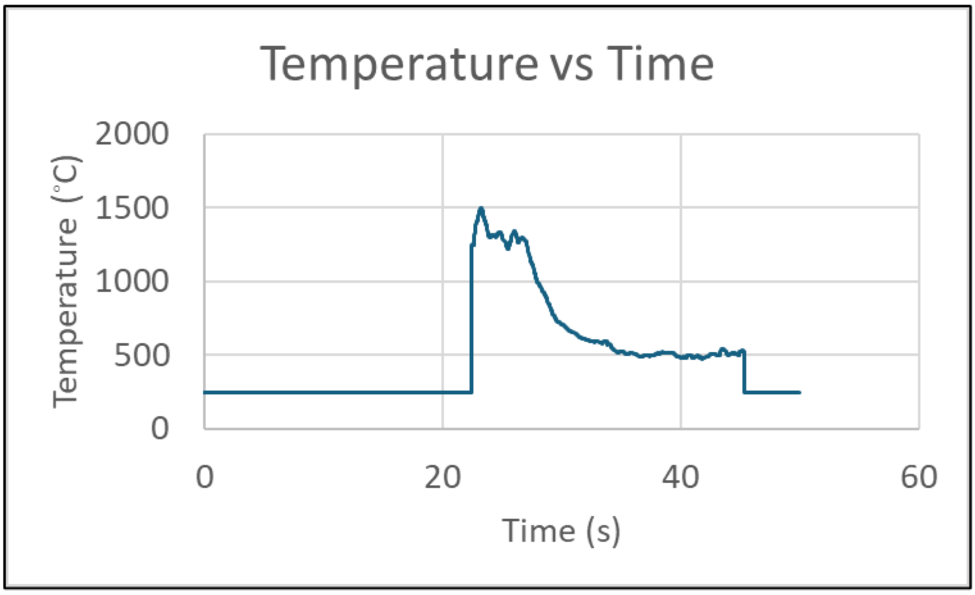

Fig. 50: Temperature vs time graph in WAAM-MIG for 680 W power

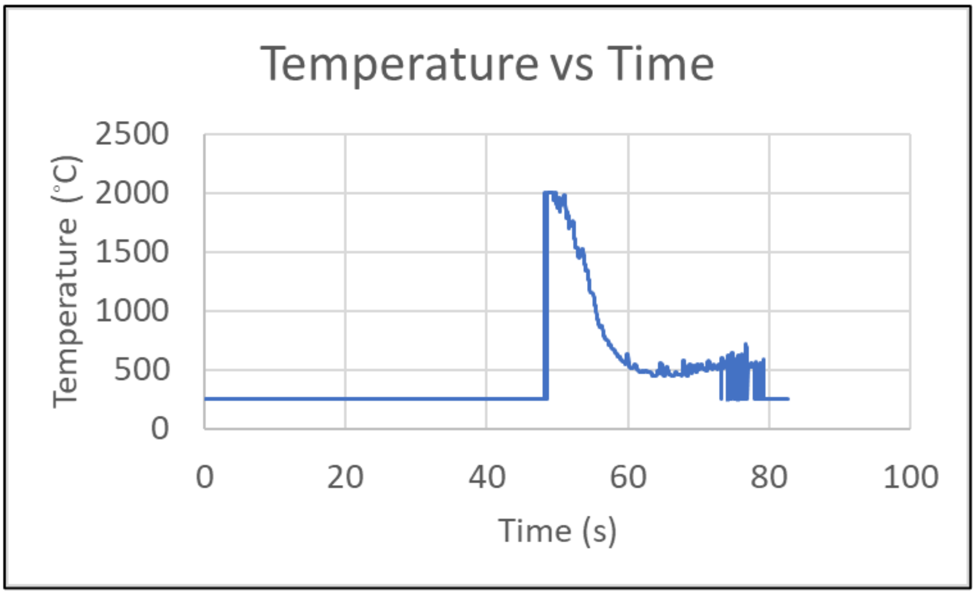

Fig. 51: Temperature vs time graph in WAAM-MIG for 738 W power

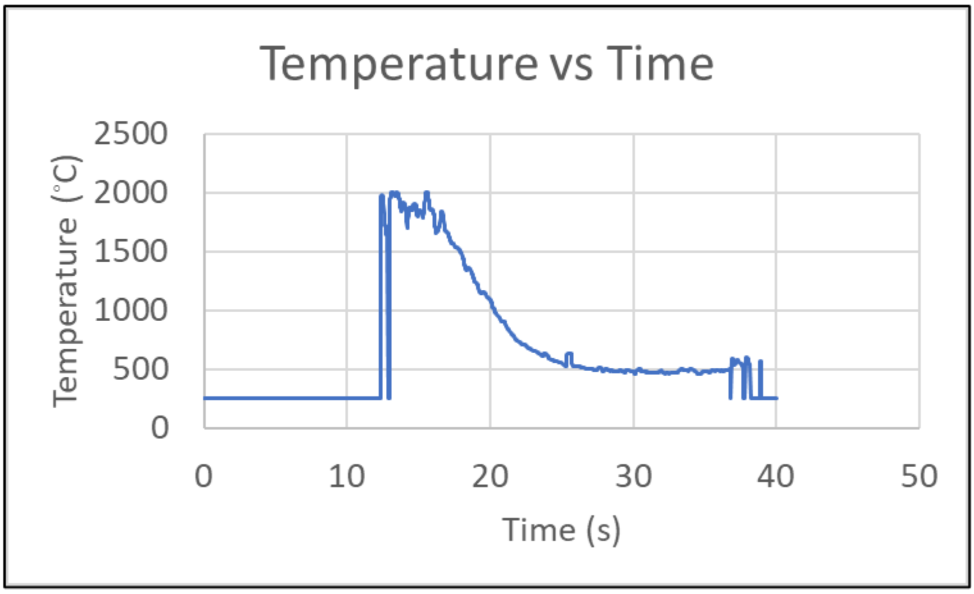

Fig. 52: Temperature vs time graph in WAAM-MIG for 779 W power

From the temperature vs time graph cooling rate is calculated which is shown in the table below.

Table 13: Cooling rate calculated for each deposited bead using WAAM-MIG process

Power (W)	Cooling Rate (°C/s)
680	37.36
738	39.37
779	41.32

A graph is plotted between cooling rate vs power is plotted.

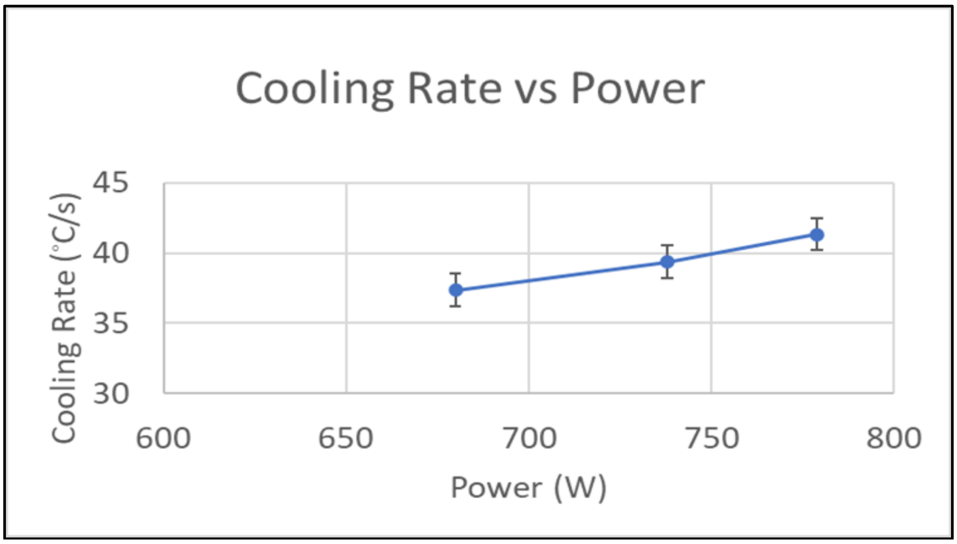

Fig. 53: Cooling rate vs power for WAAM-MIG depositions

7.4 Specific energy

Specific energy is calculated as per eq.3.3 and a graph is being plotted between specific energy vs power.

Table 14: Specific energy calculated for each power level of the WAAM-MIG deposition

Power (W)	Specific Energy (J/mm^3)
680	40.58
738	44.04
779	46.49

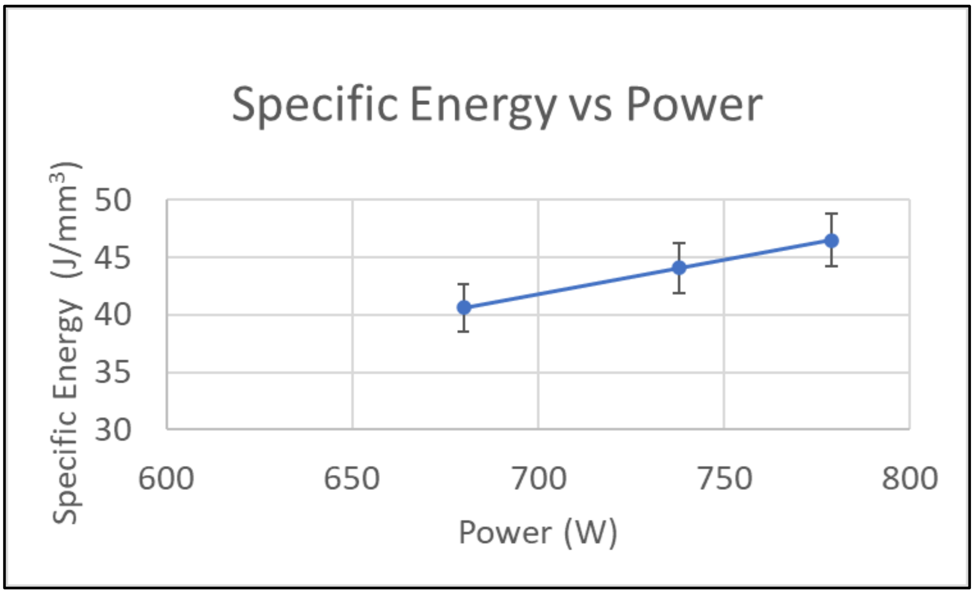

Fig. 54: Specific energy vs power for WAAM-MIG depositions

7.5 Output parameters

The output parameters are bead width, bead height and hardness which are measured after the three linear deposition the bead height, bead width and hardness are measured.

7.5.1 Bead width and bead height measurement

The bead width and bead height are measured using LDS. The width and height are measured from 40 mm from start, 50 mm from start and 60 mm from start. Then average of the values are taken and noted down.

Table 15: Bead width and bead height of WAAM-MIG deposition

Power (W)	Bead Width (mm)				Bead Height (mm)			
	40 mm from start	50 mm from start	60 mm from start	Mean	40 mm from start	50 mm from start	60 mm from start	Mean
680	3.42	4.22	2.92	3.52	4.16	2.74	2.94	3.28
738	3.31	4.18	3.51	3.67	3.05	2.95	3.21	3.07
779	4.43	3.83	3.86	4.04	3.39	2.62	2.72	2.91

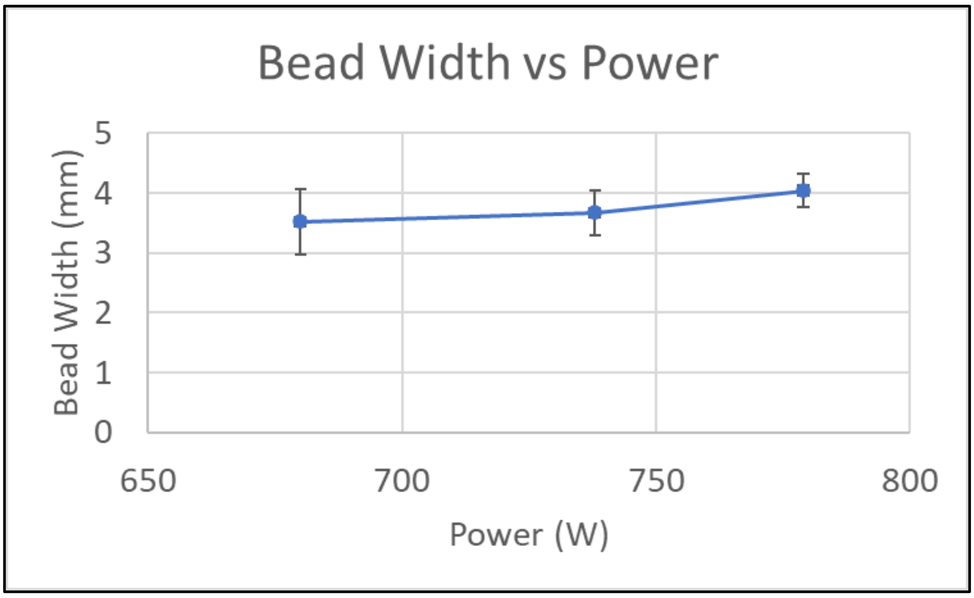

Fig. 55: Bead width vs power for WAAM-MIG depositions

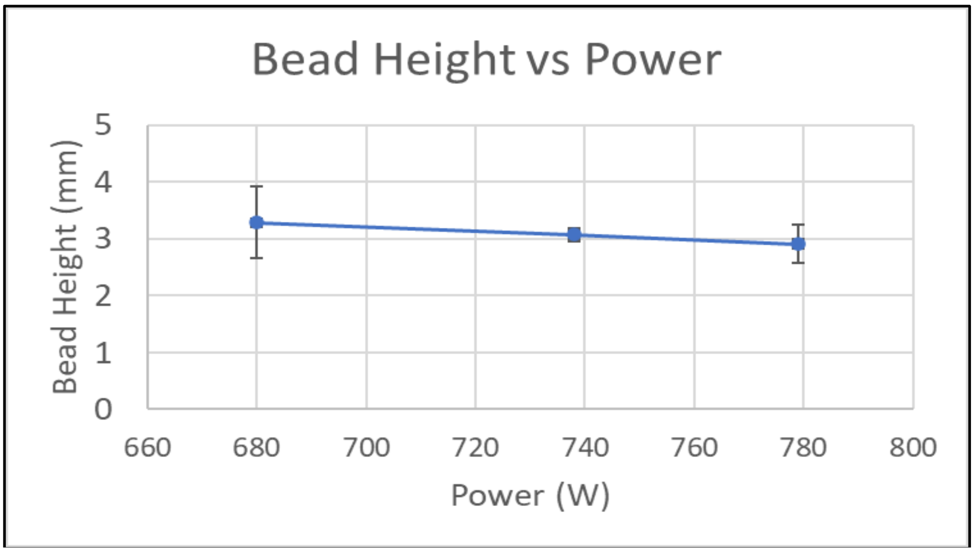

Fig. 56: Bead height vs power for WAAM-MIG depositions

7.5.2 Hardness measurement

The samples are cut using a water jet abrasive cutter along the cross section which are polished using sand paper of grit size 80 and 1000. Polishing is done upto such a level so that the samples are free from irregularities. After polishing the samples, the hardness of the samples is measured using Vickers hardness testing machine. The hardness is measured at three different positions and mean value of the readings are noted. Load of 0.3 kg is used at a dwell time of 10 s. The hardness is measured using the eq. 3.1.

Fig. 57: Cut cross of the polished WAAM-MIG weld bead,
(a) 680 W, (b) 738 W, (c) 779 W

Table 16: Hardness of deposited beads in WAAM-MIG process

Power (W)	Hardness
680	285.43
738	288.56
779	289.53

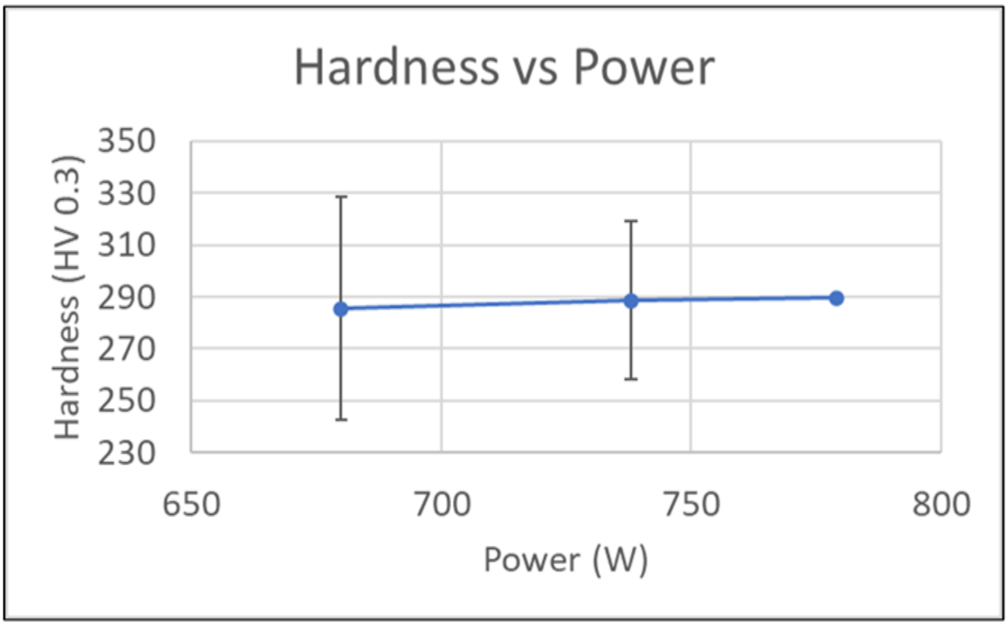

Fig. 58: Hardness vs power for WAAM-MIG depositions

Chapter 8
Results and Discussion for Laser-TIG Hybrid Additive Manufacturing

In Laser-TIG Hybrid Additive Manufacturing (LTHAM) the input parameters are wire feed speed, deposition speed and power. Wire feed speed and deposition speed are kept constant. The power is varied for doing the depositions. Three linear depositions of length 100 mm are being done. The TIG torch is kept at 25° with respect to the workpiece. The laser is held perpendicular to the workpiece. While deposition both the laser as well as TIG are switched on simultaneously.

8.1 Input parameters

Table 17: Input parameters used in Laser-TIG hybrid depositions

TIG Power (W)	480	720	960
Laser Power (W)	1200		
Wire Feed Speed (m/min)	2		
Deposition Speed (mm/min)	100		

8.2 Laser-TIG hybrid depositions

Three linear single layer depositions are done using Laser-TIG hybrid as shown in the figures below.

Fig. 59: LTHAM deposition for TIG power : 480 W and Laser power : 1200 W

Fig. 60: LTHAM deposition for TIG power : 720 W and Laser power : 1200 W

Fig. 61: LTHAM deposition for TIG power : 960 W and Laser power : 1200 W

8.3 Temperature recording for each deposition and measurement of cooling rate

Temperature is recorded during the deposition which is obtained in the form of temperature and time. Cooling rate is calculated using the eq.3.2.

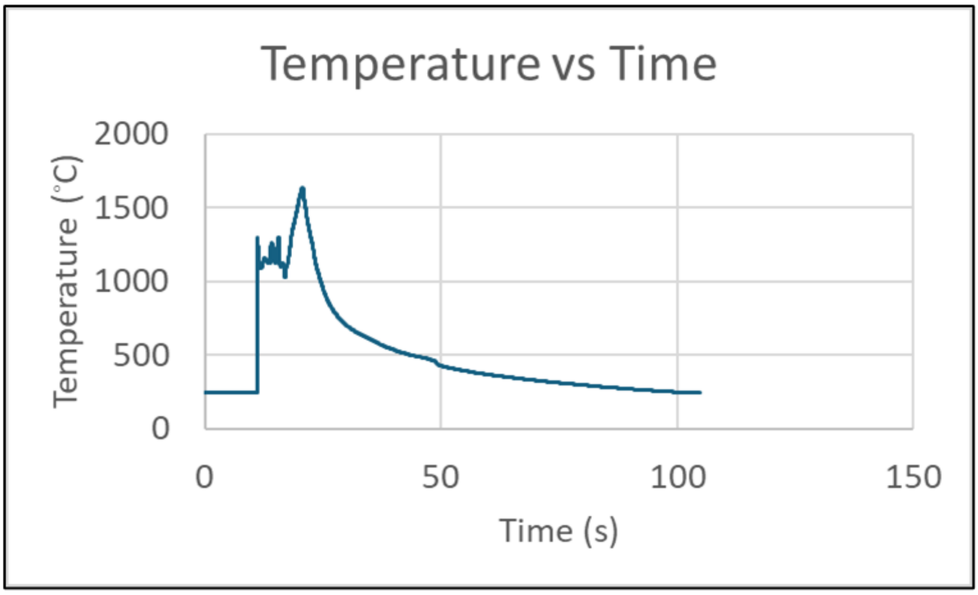

Fig. 62: Temperature vs time graph in Laser-TIG hybrid deposition for TIG power 480 W and laser power 1200 W

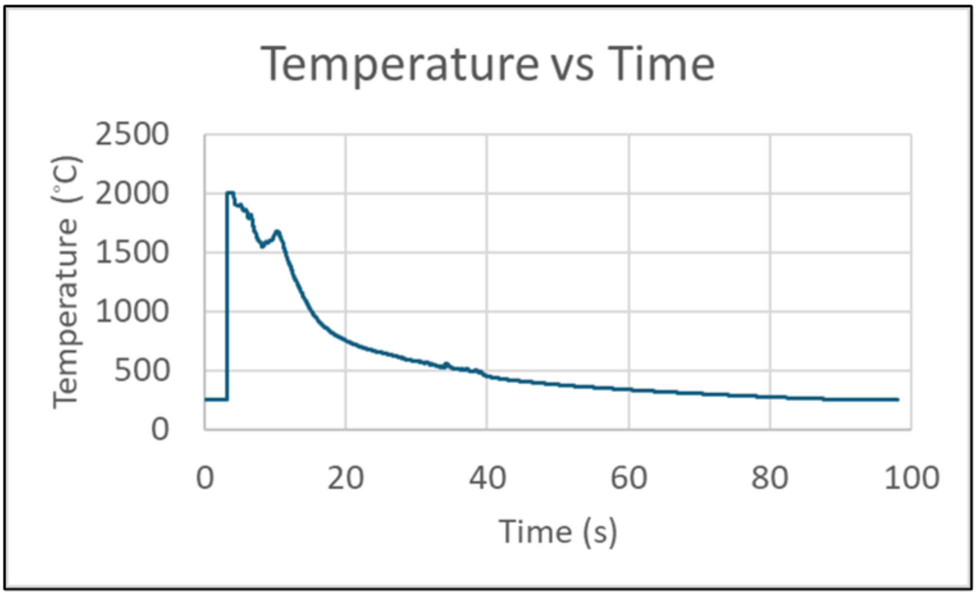

Fig. 63: Temperature vs time graph in Laser-TIG hybrid deposition for TIG power 720 W and laser power 1200 W

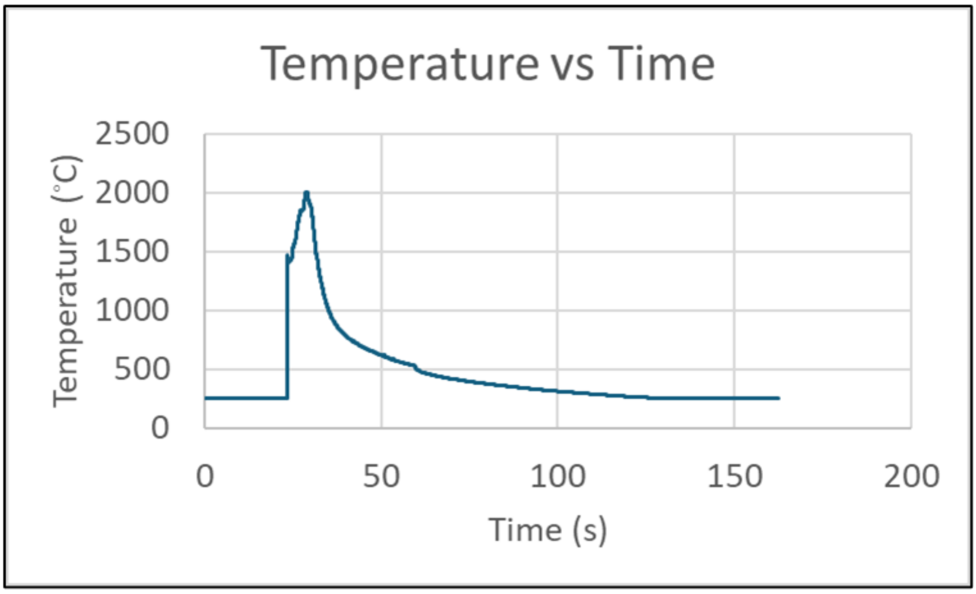

Fig. 64: Temperature vs time graph in Laser-TIG hybrid deposition for TIG power 960 W and laser power 1200 W

From the temperature vs time graph cooling rate is calculated which is shown in the table below.

Table 18: Cooling rate calculated for each deposited bead using Laser-TIG hybrid process

TIG Power (W)	Laser Power (W)	Cooling Rate (°C/s)
480	1200	27.15
720		16.42
960		9.55

A graph is plotted between cooling rate vs power is plotted.

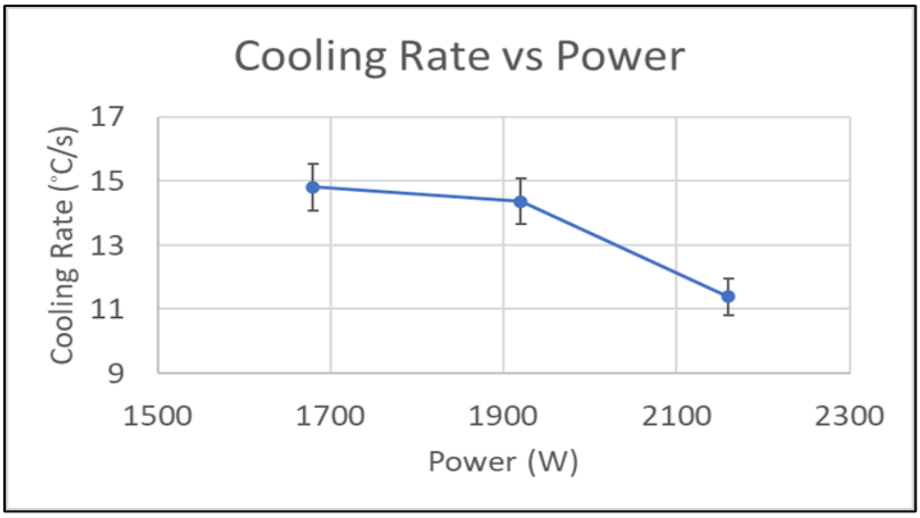

Fig. 65: Cooling rate vs power for Laser-TIG hybrid depositions

8.4 Specific energy

Specific energy is calculated as per eq.3.3 and a graph is being plotted between specific energy vs power.

Table 19: Specific energy calculated for each power level of the Laser-TIG hybrid deposition

TIG Power (W)	Laser Power (W)	Specific Energy (J/mm^3)
480	1200	100.29
720		114.62
960		128.95

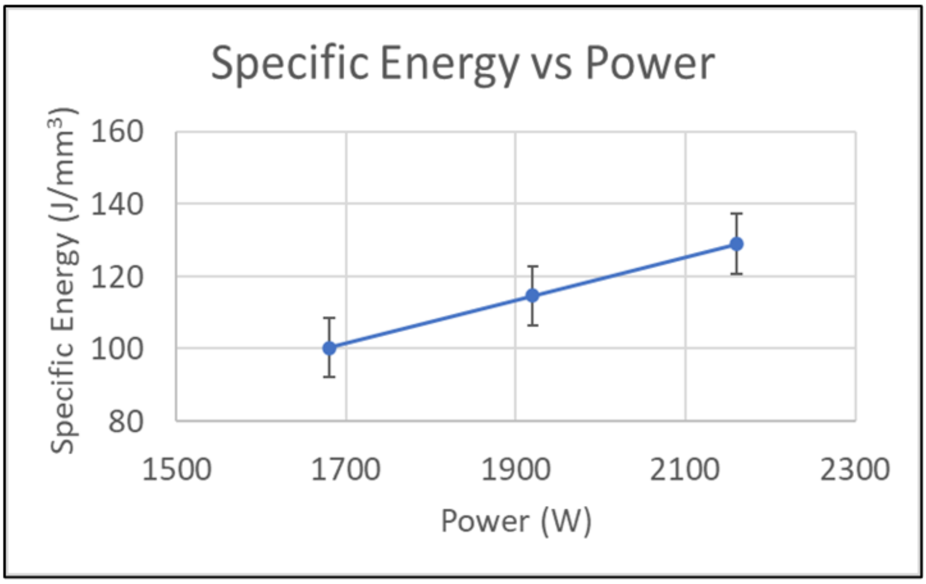

Fig. 66: Specific energy vs power for Laser-TIG hybrid depositions

8.5 Output parameters

The output parameters are bead width, bead height and hardness which are measured after the three linear depositions the bead height, bead width and hardness are measured.

8.5.1 Bead width and bead height measurement

The bead width and bead height are measured using LDS. The width and height are measured from 40 mm from start, 50 mm from start and 60 mm from start. Then average of the values are taken and noted down.

Table 20: Bead width and bead height of Laser-TIG hybrid deposited beads

Laser Power (W)	TIG Power (W)	Bead Width (mm)				Bead Height (mm)			
		40 mm from start	50 mm from start	60 mm from start	Mean	40 mm from start	50 mm from start	60 mm from start	Mean
1200	480	3.91	3.85	4.45	4.07	2.83	2.51	2.73	2.69
	720	4.23	4.37	4.12	4.24	2.44	2.41	2.35	2.4
	960	6.79	6.76	6.97	6.84	1.71	2.00	1.96	1.89

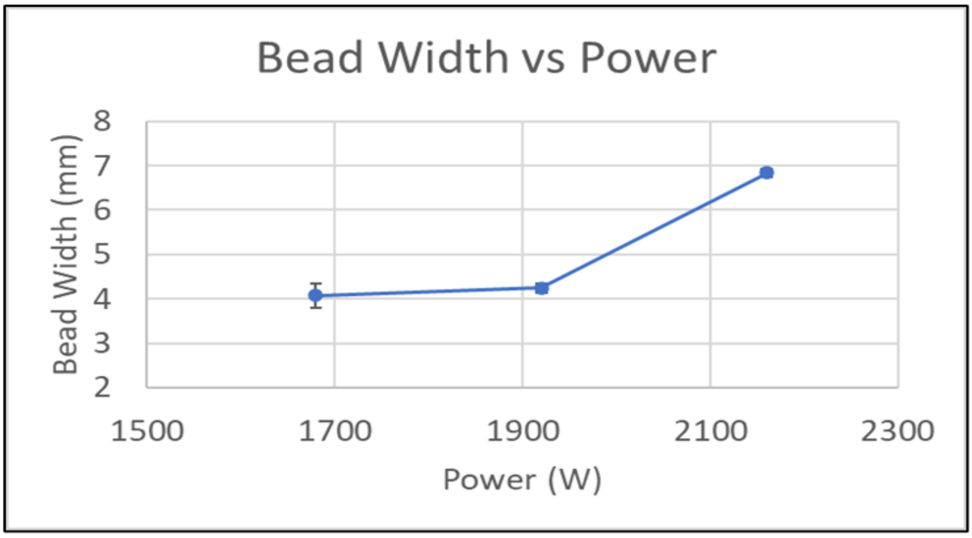

Fig. 67: Bead width vs power for Laser-TIG hybrid depositions

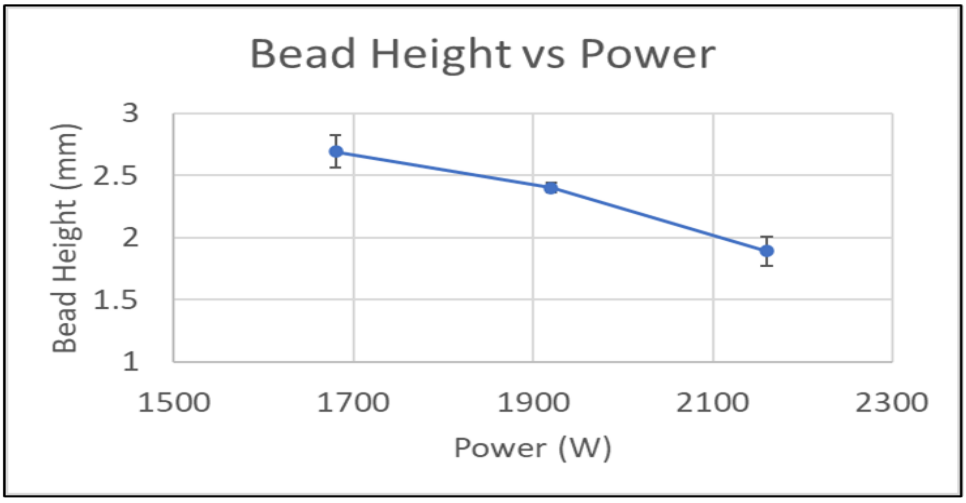

Fig. 68: Bead height vs power for Laser-TIG hybrid depositions

8.5.2 Hardness measurement

The samples are cut using a water jet abrasive cutter along the cross section, which are polished using sand paper of grit size 80 and 1000. Polishing is done upto such a level so that the samples are free from irregularities. After polishing the samples, the hardness of the samples is measured using Vickers hardness testing machine. The hardness is measured at three different positions and mean value of the readings are noted. Load of 0.3 kg is used at a dwell time of 10 s. Hardness is measured using the eq. 3.1.

Fig. 69: Cut cross of the polished Laser-TIG hybrid weld bead,
(a) Laser power 1200 W and TIG power 480 W ,
(b) Laser power 1200 W and TIG power 720 W,
(c) Laser power 1200 W and TIG power 960 W

Table 21: Hardness of deposited beads in Laser-TIG hybrid process

TIG Power (W)	Laser Power (W)	Hardness
480	1200	289.1
720		270.13
960		260.13

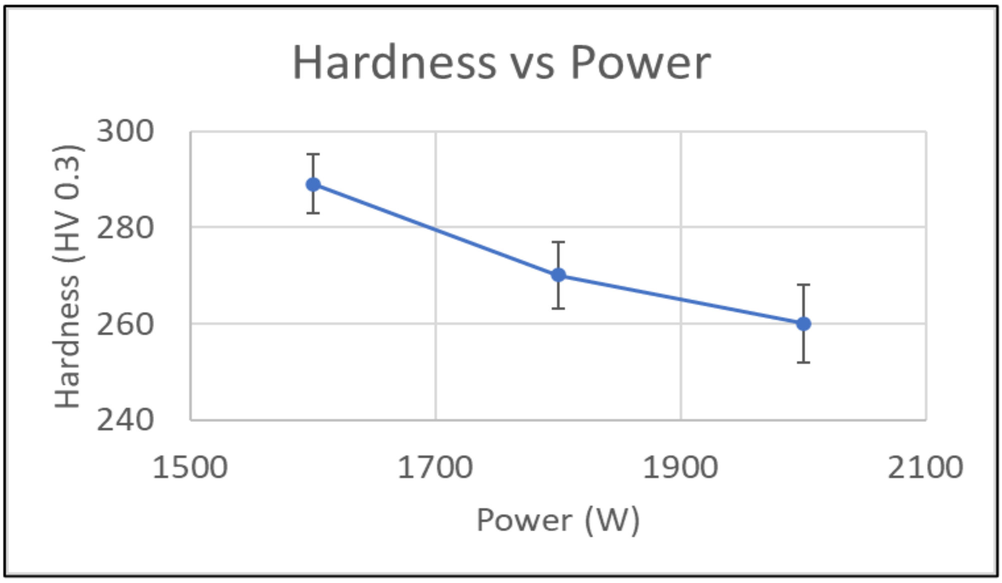

Fig. 70: Hardness vs power for Laser-TIG hybrid depositions

Chapter 9
Results and Discussion for MIG-TIG Hybrid Additive Manufacturing

In MIG-TIG Hybrid Additive Manufacturing (MTHAM) the input parameters are wire feed speed, deposition speed and power. Wire feed speed and deposition speed are kept constant. The power is varied for doing the depositions. Three linear depositions of length 100 mm are being done. The TIG torch is kept at 65° with respect to the workpiece. The laser is held perpendicular to the workpiece. While deposition both the MIG as well as TIG torch are switched on simultaneously.

9.1 Input parameters

Table 22: Input parameters used in MIG-TIG hybrid depositions

TIG Power (W)	360	480	720
MIG Power (W)	300		
Wire Feed Speed (m/min)	2		
Deposition Speed (mm/min)	100		

9.2 MIG-TIG hybrid depositions

Three linear single layer depositions are done using MIG-TIG hybrid as shown in the figures below.

Fig. 71: MTHAM deposition for TIG power 360 W and MIG power 300 W

Fig. 72: MTHAM deposition for TIG power 480 W and MIG power 300 W

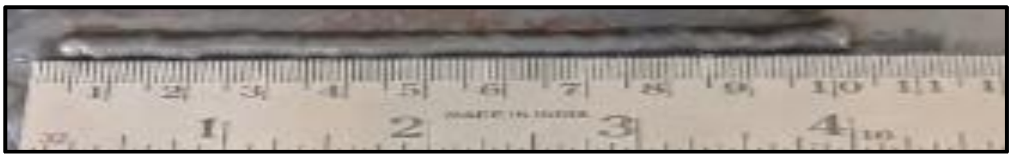

Fig. 73: MTHAM deposition for TIG power 720 W and MIG power 300 W

9.3 Temperature recording for each deposition and measurement of cooling rate

Temperature is recorded during the deposition which is obtained in the form of temperature and time. Cooling rate is calculated using the eq.3.2.

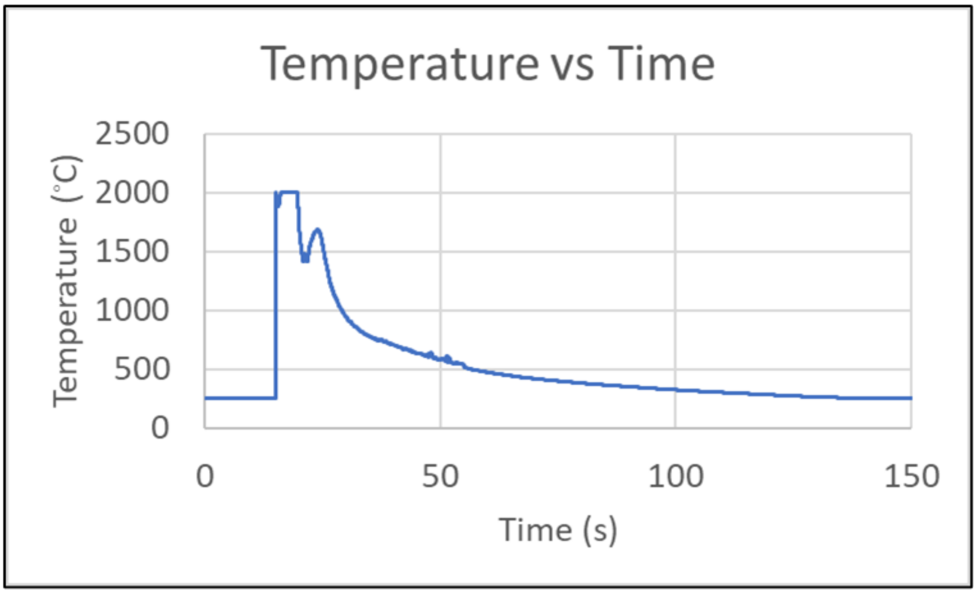

Fig. 74: Temperature vs time graph in MIG- TIG hybrid deposition for TIG power 360 W and MIG power 300 W

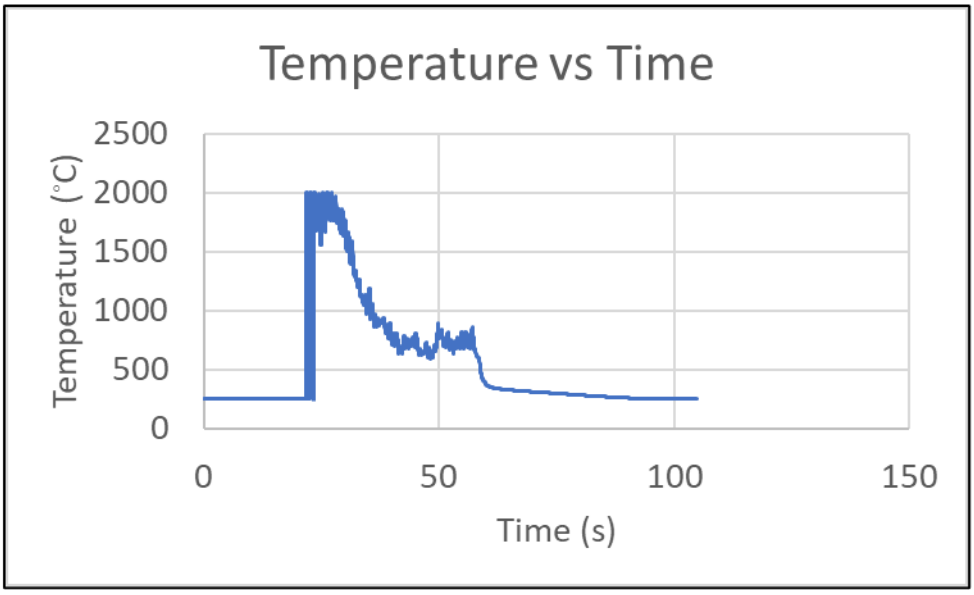

Fig. 75: Temperature vs time graph in MIG-TIG hybrid deposition for TIG power 480 W and MIG power 300 W

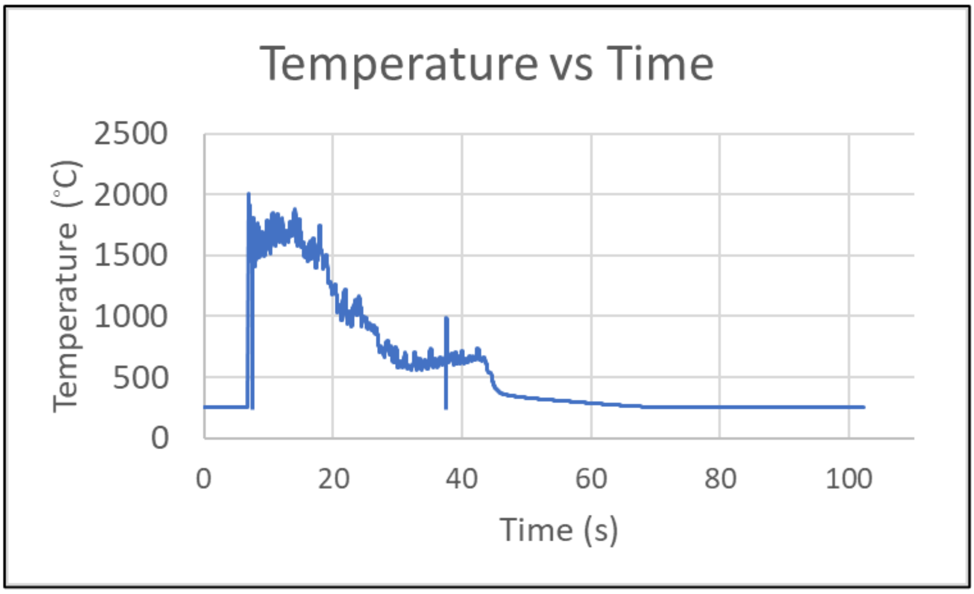

Fig. 76: Temperature vs time graph in MIG-TIG hybrid deposition for TIG power 720 W and MIG power 300 W

From the temperature vs time graph cooling rate is calculated which is shown in the table below.

Table 23: Cooling rate calculated for each deposited bead using MIG-TIG hybrid process

TIG Power (W)	MIG Power (W)	Cooling Rate (°C/s)
360	300	9.98
480		18.03
720		22.4

A graph is plotted between cooling rate vs power is plotted.

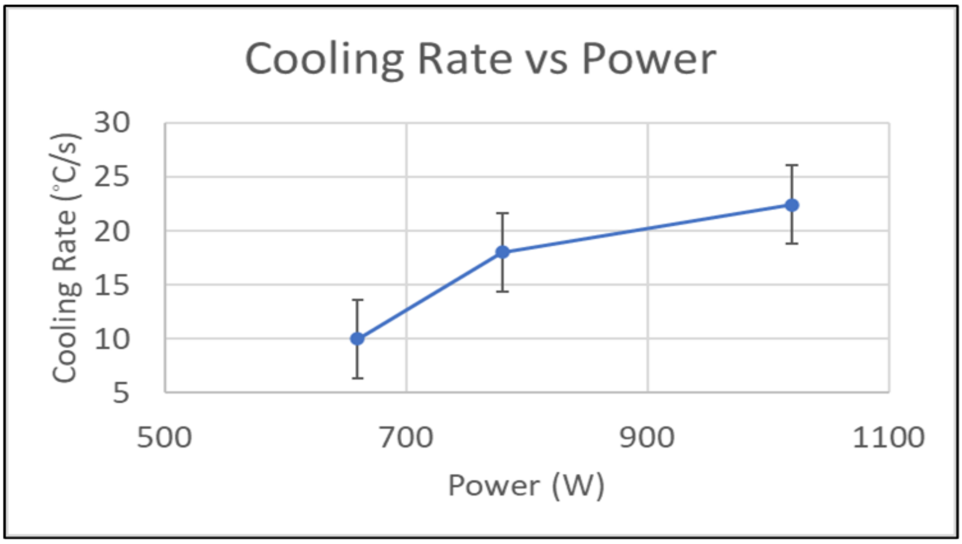

Fig. 77: Cooling rate vs power for MIG-TIG hybrid depositions

9.4 Specific energy

Specific energy is calculated as per eq.3.3 and a graph is being plotted between specific energy vs power.

Table 24: Specific energy calculated for each power level of the MIG-TIG hybrid deposition

TIG Power (W)	MIG Power (W)	Specific Energy (J/mm^3)
360	300	39.39
480		46.55
720		60.87

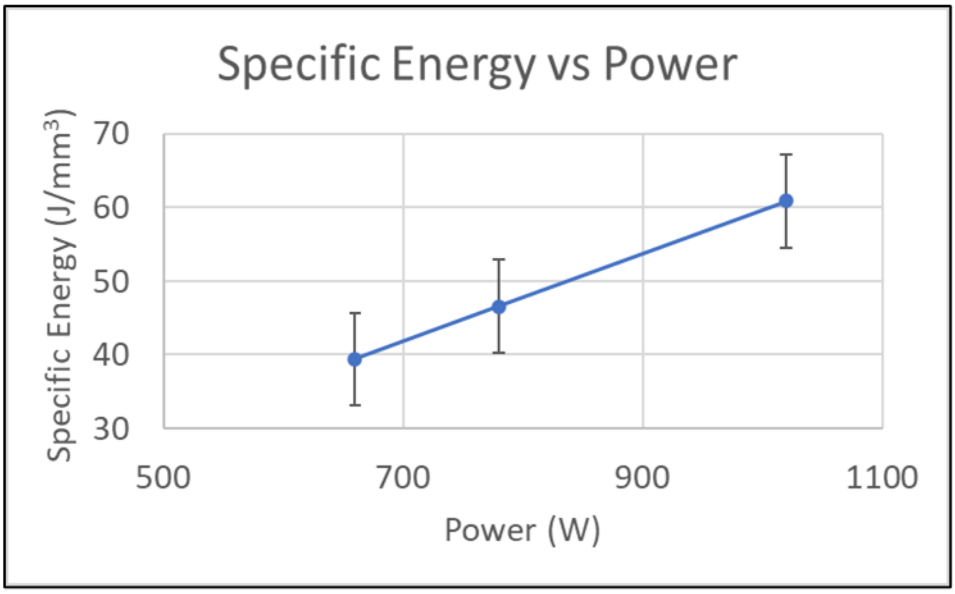

Fig. 78: Specific energy vs power for MIG-TIG hybrid depositions

9.5 Output parameters

The output parameters are bead width, bead height and hardness which are measured after the three linear depositions the bead height, bead width and hardness are measured.

9.5.1 Bead width and bead height measurement

The bead width and bead height are measured using LDS. The width and height are measured from 40 mm from start, 50 mm from start and 60 mm from start. Then average of the values are taken and noted down.

Table 25: Bead width and bead height of MIG-TIG hybrid deposited beads

MIG Power (W)	TIG Power (W)	Bead Width (mm)				Bead Height (mm)			
		40 mm from start	50 mm from start	60 mm from start	Mean	40 mm from start	50 mm from start	60 mm from start	Mean
300	360	2.27	2.53	2.66	2.48	2.13	2.96	3.08	2.72
	480	3.34	4.01	3.48	3.61	2.67	2.21	2.55	2.47
	720	3.10	4.01	3.85	3.65	2.01	2.81	2.47	2.43

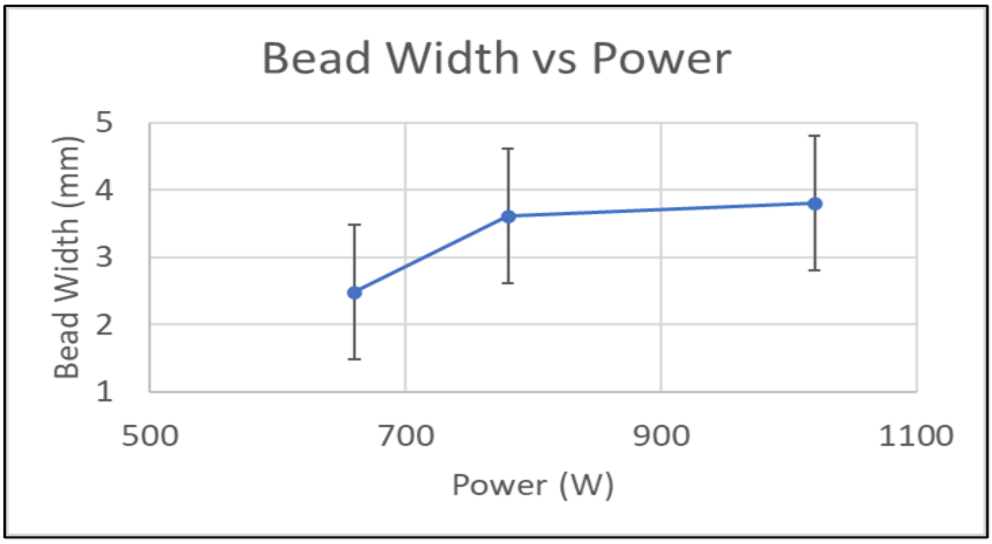

Fig. 79: Bead width vs power for MIG-TIG hybrid depositions

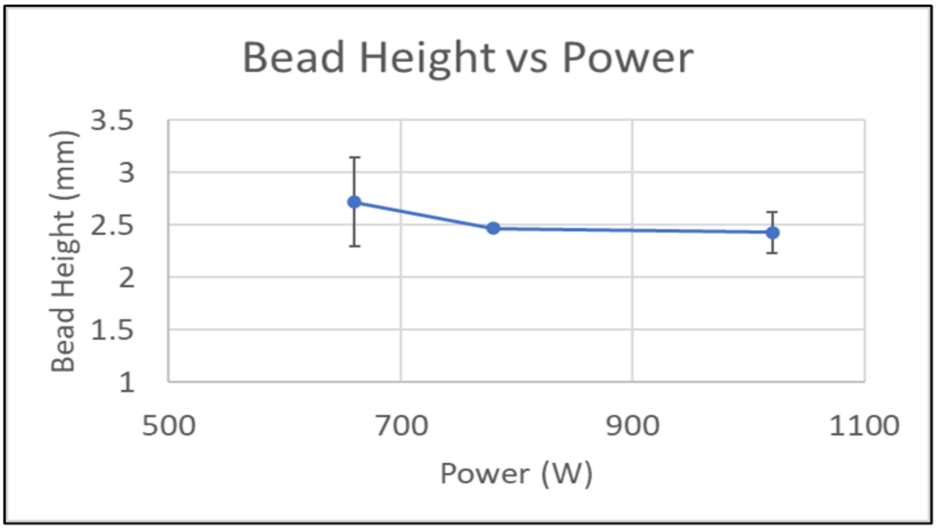

Fig. 80: Bead height vs power for MIG-TIG hybrid depositions

9.5.2 Hardness measurement

The samples are cut using a water jet abrasive cutter along the cross section, which are polished using sand paper of grit size 80 and 1000. Polishing is done upto such a level so that the samples are free from irregularities. After polishing the samples, the hardness of the samples is measured using Vickers hardness testing machine. The hardness is measured at three different positions and mean value of the readings are noted. Load of 0.3 kg is used at a dwell time of 10 s. Hardness is measured using the eq. 3.1.

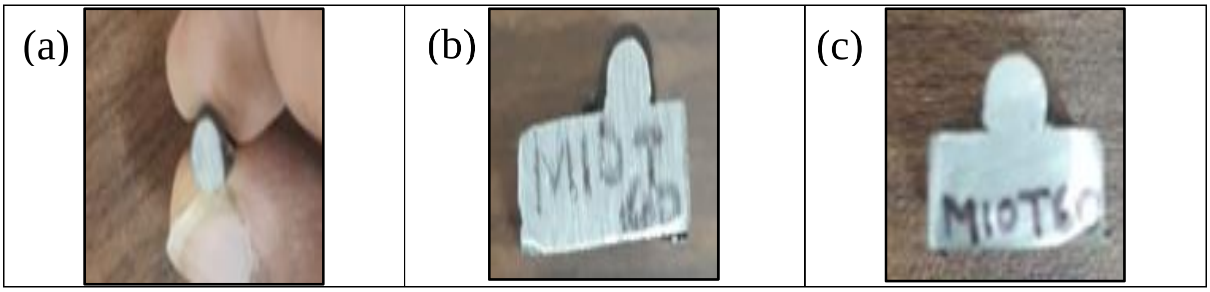

Fig. 81: Cut cross of the polished MIG-TIG hybrid weld bead,
(a) MIG power 300 W, TIG power 360 W,
(b) MIG power 300 W, TIG power 480 W,
(c) MIG power 300 W, TIG power 720 W

Table 26: Hardness of deposited beads in MIG-TIG hybrid process

TIG Power (W)	MIG Power (W)	Hardness
360	300	190.63
480		311.16
720		315.46

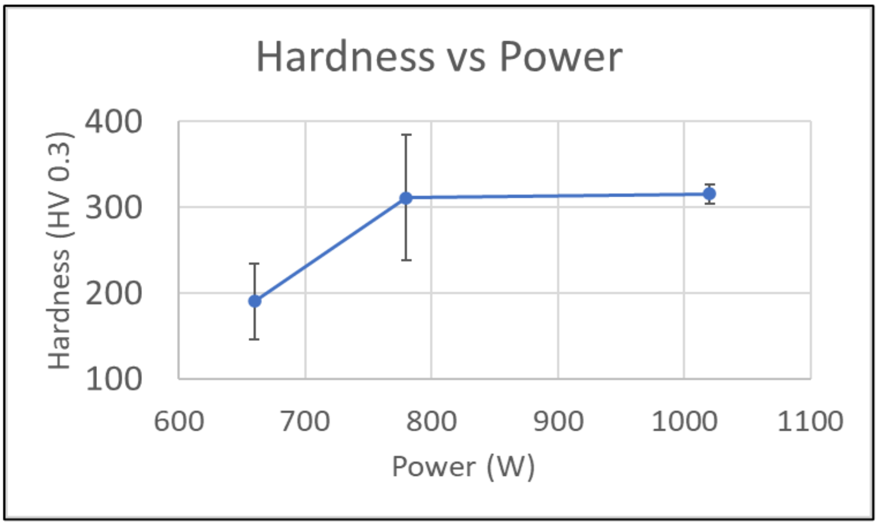

Fig. 82: Hardness vs power for MIG-TIG hybrid depositions

Chapter 10
Conclusions and Inferences

The single layer deposition were being carried out using wire Laser, wire TIG, wire MIG, Laser-TIG hybrid and MIG-TIG hybrid. During deposition, the temperature of the beads were also measured using a pyrometer. Further cooling rate and specific energy were calculated. Bead width and height of the deposited beads were measured using LDS. Hardness of the bead is also measured. The following observations were obtained :

- The cooling rate in WLAM, WAAM-MIG was found to be increasing and in the case of WAAM-TIG, Laser-TIG, MIG-TIG it was decreasing with respect to increase of power.

- The specific energy and bead width was found to be increasing with respect to increase of power in all the processes.

- However, the bead height was found to be decreasing with respect to increase of power in all the processes.

- The hardness in WLAM, WAAM-MIG and MIG-TIG hybrid additive manufacturing was found to be increasing with respect to increase of power.

- Whereas the hardness in the case of WAAM-TIG and Laser-TIG hybrid additive manufacturing was found to be decreasing with respect to increase of power.

Based on the conducted experiments and analysis various wire based additive manufacturing processes are also compared with respect to different process variants, Fig.83. The following conclusion could be drawn from this radar chart.

- Bead width is maximum in case of Laser-TIG hybrid deposition and MIG deposition whereas it is minimum in case of Laser deposition.

- Bead height is maximum in case of Laser deposition whereas it is minimum in case of Laser-TIG hybrid deposition.

- The cooling rate is maximum in case of MIG deposition whereas it is minimum in case of TIG deposition.

- Specific energy is maximum in case of Laser-TIG hybrid deposition whereas it is minimum in case of MIG-TIG hybrid deposition and MIG deposition.

- Hardness is maximum in the case of MIG-TIG hybrid deposition whereas it is minimum in case of Laser deposition.

The advantages of hybrid deposition are:

- At minimum power continuous bead deposition can be obtained as seen in the case of MIG-TIG hybrid deposition.

- ➢ The hardness of the bead is maximum as obtained in case of MIG-TIG hybrid deposition.
- ➢ The cooling rate is relatively lower as compared to deposition using Laser, TIG and MIG.

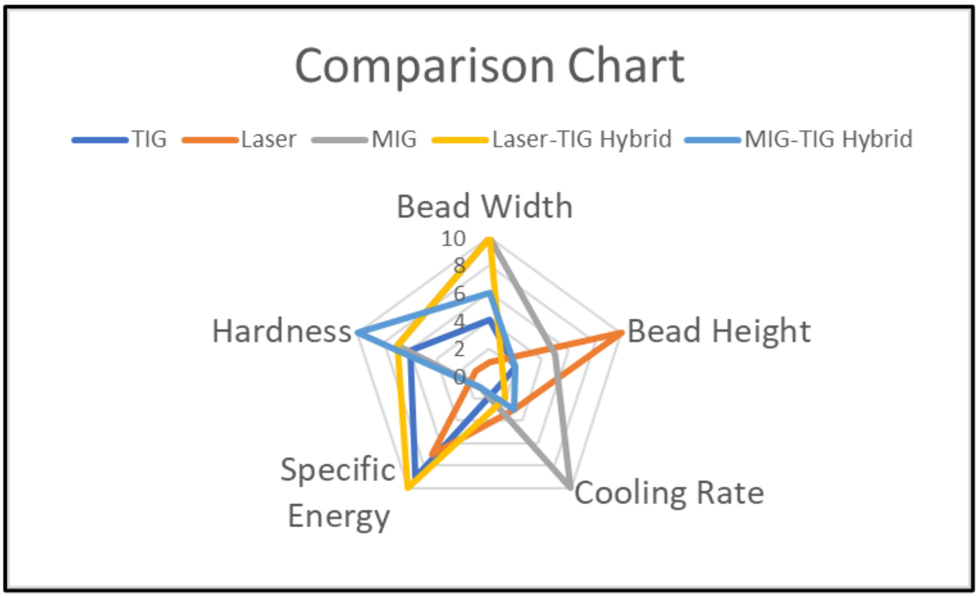

Fig. 83: Radar chart comparing various wire based additive manufacturing processes

References

1 Calignano, F., Manfredi, D., Ambrosio, E.P., Biamino, S., Lombardi, M., Atzeni, E., et al. (2017) 'Overview on additive manufacturing technologies', Proc IEEE, 105, pp. 593–612. Available at: https://doi.org/10.1109/JPROC.2016.2625098.

2 Guo, N. and Leu, M.C. (2013) 'Additive manufacturing: Technology, applications and research needs', Front Mech Eng, 8, pp. 215–243. Available at: https://doi.org/10.1007/s11465-013-0248-8.

3 Horst, D., Duvoisin, C., & Vieira, R. (2018) 'Additive Manufacturing at Industry 4.0: a Review', Int J Eng Tech Res, 8, pp. 3–8.

4 Pan, Z., Ding, D., Wu, B., Cuiuri, D., Li, H., & Norrish, J. (2018) 'Arc Welding Processes for Additive Manufacturing: A Review', Transactions on Intelligent Welding Manufacturing, pp. 3–24. Available at: https://doi.org/10.1007/978-981-105355-9.

5 Feng, Z. (2005) Processes and Mechanisms of Welding Residual Stress and Distortion. Aington: Woodhead Publishing Limited.

6 Ding, D., Pan, Z., Cuiuri, D., & Li, H. (2015) 'Wire-feed additive manufacturing of metal components: technologies, developments and future interests', International Journal of Advanced Manufacturing Technology, 81, pp. 465–481. Available at: https://doi.org/10.1007/s00170-015-7077-3.

7 Ding, D., Pan, Z., Cuiuri, D., & Li, H. (2015) 'A practical path planning methodology for wire and arc additive manufacturing of thin-walled structures', Robotics and Computer Integrated Manufacturing, 34, pp. 8–19. Available at: https://doi.org/10.1016/j.rcim.2015.01.003.

8 Pan, Z., Ding, D., Wu, B., Cuiuri, D., Li, H., & Norrish, J. (2018) 'Arc Welding Processes for Additive Manufacturing: A Review', in Transactions on Intelligent Welding Manufacturing, pp. 3–24. Available at: https://doi.org/10.1007/978-981-105355-9.

9 Williams, S.W., Martina, F., Addison, A.C., Ding, J., Pardal, G., & Colegrove, P. (2016) 'Wire + Arc additive manufacturing', Materials Science and Technology, 32, pp. 641–647. Available at: https://doi.org/10.1179/1743284715Y.0000000073.

10 Wu, B., Pan, Z., Ding, D., Cuiuri, D., Li, H., Xu, J., et al. (2018) 'A review of the wire arc additive manufacturing of metals: properties, defects and quality improvement', Journal of Manufacturing Process, 35, pp. 127–139. Available at: https://doi.org/10.1016/j.jmapro.2018.08.001.

11 Ding, D., Pan, Z., van Duin, S., Li, H., & Shen, C. (2016) 'Fabricating superior NiAl bronze components through wire arc additive manufacturing', Materials, 9. Available at: https://doi.org/10.3390/ma9080652.

12 Abuabiah, M., Mbodj, N.G., Shaqour, B., Herzallah, L., Juaidi, A., Abdallah, R., & Plapper, P. (2023) 'Advancements in Laser Wire-Feed Metal Additive Manufacturing: A Brief Review', Materials, 16(5), 2030. Available at: https://doi.org/10.3390/ma16052030.

13 UTI. (n.d.) 'GMAW (MIG) Welding', UTI Blog. Available at: https://www.uti.edu/blog/welding/gmaw-mig-welding.

14 Asadi, P., Kazemi-Choobi, K., & Elhami, A. (Year of publication not provided) 'Welding of Magnesium Alloys'. Available at: http://dx.doi.org/10.5772/47849.

15 Weis, S., Grunert, R., Brumm, S., Halmaghi, M., & Prank, U. (2023) 'Comparative study between TIG-MIG hybrid and MIG welding of 1.4462 duplex steel joints', Welding in the World, 68, pp. 51–59. Available at: https://doi.org/10.1007/s40194-023-01620-5.

16 Herzog, D., Seyda, V., Wycisk, E., & Emmelmann, C. (2016) 'Additive manufacturing of metals', Acta Materialia, 117, pp. 371–392. Available at: https://doi.org/10.1016/j.actamat.2016.07.019.

17 Tapia, G., & Elwany, A. (2014) 'A Review on Process Monitoring and Control in Metal-Based

Additive Manufacturing', Journal of Manufacturing Science and Engineering, Trans ASME, 136. Available at: https://doi.org/10.1115/1.4028540.
18 Karpagaraj, A., Siva Shanmugam, N., & Sankaranarayanasamy, K. (2015) 'Some studies on mechanical properties and microstructural characterisation of automated TIG welding of thin commercially pure titanium sheets', Materials Science and Engineering: A, 640, pp. 180–189. Available at: https://doi.org/10.1016/j.msea.2015.05.056.
19 Norman, A.F., Drazhner, V., & Prangnell, P.B. (1999) 'Effect of welding parameters on the solidification microstructure of autogenous TIG welds in an Al-CuMg-Mn alloy', Materials Science and Engineering: A, 259, pp. 53–64. Available at: https://doi.org/10.1016/S0921-5093(98)00873-9.
20 Mirshekari, G.R., Tavakoli, E., Atapour, M., & Sadeghian, B. (2014) 'Microstructure and corrosion behavior of multipass gas tungsten arc welded 304L stainless steel', Materials & Design, 55, pp. 905–911. Available at: https://doi.org/10.1016/j.matdes.2013.10.064.
21 Lv, S.X., Jing, X.J., Huang, Y.X., Xu, Y.Q., Zheng, C.Q., & Yang, S.Q. (2012) 'Investigation on TIG arc welding-brazing of Ti/Al dissimilar alloys with Al based fillers', Science and Technology of Welding and Joining, 17, pp. 519–524. Available at: https://doi.org/10.1179/1362171812Y.0000000041.
22 Nandagopal, K., & Kailasanathan, C. (2016) 'Analysis of mechanical properties and optimization of gas tungsten Arc welding (GTAW) parameters on dissimilar metal titanium (6Al-4V) and aluminium 7075 by Taguchi and ANOVA techniques', Journal of Alloys and Compounds, 682, pp. 503–516. Available at: https://doi.org/10.1016/j.jallcom.2016.05.006.
23 Kumar, R., Ghosh, P.K., & Kumar, S. (2017) 'Thermal and metallurgical characteristics of surface modification of AISI 8620 steel produced by TIG arcing process', Journal of Materials Processing Technology, 240, pp. 420–431. Available at: https://doi.org/10.1016/j.jmatprotec.2016.10.020.

24 Kumar, S., Ghosh, P.K., & Kumar, R. (2017) 'Surface modification of AISI 4340 steel by multi-pass TIG arcing process', Journal of Materials Processing Technology, 249, pp. 394–406. Available at: https://doi.org/10.1016/j.jmatprotec.2017.06.035.
25 Lin, C.M., Chang, C.M., Chen, J.H., Hsieh, C.C., & Wu, W. (2010) 'Microstructure and wear characteristics of high-carbon Cr-based alloy claddings formed by gas tungsten arc welding (GTAW)', Surface and Coatings Technology, 205, pp. 2590–2596. Available at: https://doi.org/10.1016/j.surfcoat.2010.10.004.
26 Advanced Energy. (n.d.) Advanced energy. Available at: https://www.advancedenergy.com/globalassets/resourcesroot/manuals/en-op-igar-6-advanced-manual.pdf.
27 Lv, S.X., Xu, Z.W., Wang, H.T., & Yang, S.Q. (2008) 'Investigation on TIG cladding of copper alloy on steel plate', Science and Technology of Welding and Joining, 13, pp. 10–16. Available at: https://doi.org/10.1179/174329307X249414.
28 Sahoo, C.K., & Masanta, M. (2017) 'Microstructure and mechanical properties of TiC-Ni coating on AISI304 steel produced by TIG cladding process', Journal of Materials Processing Technology, 240, pp. 126–137. Available at: https://doi.org/10.1016/j.jmatprotec.2016.09.018.
29 Amirsadeghi, A., & Sohi, M.H. (2008) 'Comparison of the influence of molybdenum and chromium TIG surface alloying on the microstructure, hardness and wear resistance of ADI', Journal of Materials Processing Technology, 201, pp. 673–677. Available at: https://doi.org/10.1016/j.jmatprotec.2007.11.157.
30 Ulutan, M., Yildirim, M.M., Buytoz, S., & Çelik, O.N. (2011) 'Microstructure and wear behavior of TIG surface-alloyed AISI 4140 steel', Tribology Transactions, 54, pp. 67–79. Available at: https://doi.org/10.1080/10402004.2010.519859.

31 Karamiş, M.B., & Yildizli, K. (2010) 'Surface modification of nodular cast iron: A comparative study on graphite elimination', Materials Science and Engineering: A, 527, pp. 5225–5229. Available at: https://doi.org/10.1016/j.msea.2010.04.067.

32 Ulutan, M., Yildirim, M.M., Buytoz, S., & Çelik, O.N. (2011) 'Microstructure and wear behavior of TIG surface-alloyed AISI 4140 steel', Tribology Transactions, 54, pp. 67–79. Available at: https://doi.org/10.1080/10402004.2010.519859.

33 Orłowicz, A.W., Trytek, A., Korzeniowski, M., & Kupiec, B. (2018) 'Surface hardening of nodular cast iron by GTAW remelting', Archives of Foundry Engineering, 18, pp. 53–58. Available at: https://doi.org/10.24425/123601.

34 Karamiş, M.B., & Yildizli, K. (2010) 'Surface modification of nodular cast iron: A comparative study on graphite elimination', Materials Science and Engineering: A, 527, pp. 5225–5229. Available at: https://doi.org/10.1016/j.msea.2010.04.067.

35 Lv, S.X., Xu, Z.W., Wang, H.T., & Yang, S.Q. (2008) 'Investigation on TIG cladding of copper alloy on steel plate', Science and Technology of Welding and Joining, 13, pp. 10–16. Available at: https://doi.org/10.1179/174329307X249414.

36 Bi, G., Gasser, A., Wissenbach, K., Drenker, A., & Poprawe, R. (2006) 'Identification and qualification of temperature signal for monitoring and control in laser cladding', Optics and Lasers in Engineering, 44, pp. 1348–1359. Available at: https://doi.org/10.1016/j.optlaseng.2006.01.009.

37 Liberini, M., Astarita, A., Campatelli, G., Scippa, A., Montevecchi, F., Venturini, G., Durante, M., Boccarusso, L., Memola, F., Minutolo, C., & Squillace, A. (2017) 'Selection of optimal process parameters for wire arc additive manufacturing', Procedia CIRP, 62, pp. 470-474. Available at: https://doi.org/10.1016/j.procir.2016.06.124.

38 Panchenko, I., Gudala, S., Labunskii, D., & Konovalov, S. (2024) 'Microstructural evolution and the effect of electron beam melting on the fatigue characteristics of 7075 Al alloy deposited by MIG arc additively manufacturing', International Journal on Interactive Design and Manufacturing (IJIDeM). Available at: https://doi.org/10.1007/s12008-023-01729-3.

39 Liao, H., Zhang, W., Xie, H., Li, X., Zhang, Q., Wu, X., Tian, J., & Wang, Z. (2023) 'Effects of welding speed on welding process stability, microstructure and mechanical performance of SUS304 welded by local dry underwater pulsed MIG', Journal of Manufacturing Processes, Volume 88, pp. 84-96. Available at: https://doi.org/10.1016/j.jmapro.2023.01.047.

40 Khan, A.U., Patidar, M., & Madhukar, Y.K. (2022) 'In-Situ Temperature Monitoring and Feedback Control in the Gas Tungsten Arc Welding Process'. Available at: https://doi.org/10.1007/s12541-022-00704-4.

41 Oua, W., Mukherjee, T., Knapp, G.L., Wei, Y., & Debroy, T. (2018) 'Fusion zone geometries, cooling rates and solidification parameters during wire arc additive manufacturing'. Available at: https://doi.org/10.1016/j.ijheatmasstransfer.2018.08.111.

42 Zhao, S., Yang, L., Huang, Y., & Xu, S. (2020) 'Enrichment of in-situ synthesized WC by partial dissolution of ex-situ eutectoid-structured WC/W2C particle in the coatings produced by laser hot-wire deposition', Materials Letters, Volume 281, 128641. Available at: https://doi.org/10.1016/j.matlet.2020.128641.

43 Baghdadchi, A., Hosseini, V.A., Valiente Bermejo, M.A., Axelsson, B., Harati, E., Högström, M., & Karlsson, L. (2021) 'Wire Laser Metal Deposition Additive Manufacturing of Duplex Stainless Steel Components—Development of a Systematic Methodology', Materials, 14(23), 7170. doi: 10.3390/ma14237170.

44 Naksuk, N., Poolperm, P., Nakngoenthong, J., Printrakoon, W., & Yuttawiriya, R. (2022) 'Experimental investigation of hot-wire laser deposition for the additive manufacturing of titanium parts', Materials Research Express, 9, 056515. Available at: https://doi.org/10.1088/2053-1591/ac6ec2.

45 Zapata, A., Bernauer, C., Stadter, C., Kolb, C.G., & Zaeh, M.F. (2022) 'Investigation on the Cause-Effect Relationships between the Process Parameters and the Resulting Geometric Properties for Wire-Based Coaxial Laser Metal Deposition', Metals, 12(3), 455. Available at: https://doi.org/10.3390/met12030455.

46 Guo, C., & Long, J. (2022) 'Simulation on geometric morphology of multi-channel deposition in laser wire additive manufacturing', Journal of Physics: Conference Series, 2252, 012049. doi:10.1088/1742-6596/2252/1/012049.

47 He, J., Yokota, R., Imamiya, Y., Noriyama, K., & Sasahara, H. (2022) 'Investigation of the Microstructure of Ti6Al4V Alloy by Coaxial Double Laser Metal-Wire Deposition', Materials, 15(22), 7985. Available at: https://doi.org/10.3390/ma15227985.

48 Ding, X., Li, D., Zhang, Q., Ma, H., Yang, J., & Fan, S. (2022) 'Effect of ambient pressure on bead shape, microstructure and corrosion behavior of 4043 Al alloy fabricated by laser coaxial wire feeding additive manufacturing in vacuum environment', Optics & Laser Technology, Volume 153, 108242. Available at: https://doi.org/10.1016/j.optlastec.2022.108242.

49 Eimer, E., Suder, W., Williams, S., & Ding, J. (2020) 'Wire Laser Arc Additive Manufacture of aluminium zinc alloys', Welding in the World, 64, pp. 1313–1319. Available at: https://doi.org/10.1007/s40194-020-00872-9.

50 Abuabiah, M., Mbodj, N.G., Shaqour, B., Herzallah, L., Juaidi, A., Abdallah, R., & Plapper, P. (2023) 'Advancements in Laser Wire-Feed Metal Additive Manufacturing: A Brief Review', Materials, 16(5), 2030. Available at: https://doi.org/10.3390/ma16052030.

51 Sun, W., Shan, F., Zong, N., Dong, H., & Jing, T. (2021) 'A simulation and experiment study on phase transformations of Ti-6Al-4V in wire laser additive manufacturing', Materials & Design, Volume 207, 109843. Available at: https://doi.org/10.1016/j.matdes.2021.109843.

52 Liming, L., Jifeng, W., & Gang, S. (2004) 'Hybrid laser–TIG welding, laser beam welding and gas tungsten arc welding of AZ31B magnesium alloy', Materials Science and Engineering: A, Volume 381, Issues 1–2, pp. 129-133. Available at: https://doi.org/10.1016/j.msea.2004.04.044.

53 Bîrdeanu, A.-V., Ciuca, C., & Puicea, A. (2012) 'Pulsed LASER-(micro)TIG hybrid welding: Process characteristics', Journal of Materials Processing Technology, doi:10.1016/j.jmatprotec.2011.11.014.

54 Gao, Z., Shao, X., Jiang, P., Cao, L., Zhou, Q., Yue, C., Liu, Y., & Wang, C. (2016) 'Parameters optimization of hybrid fiber laser-arc butt welding on 316L stainless steel using Kriging model and GA', Optics & Laser Technology, Volume 83, pp. 153-162. Available at: https://doi.org/10.1016/j.optlastec.2016.04.001.

55 Yan, J., Gao, M., & Zeng, X. (2010) 'Study on microstructure and mechanical properties of 304 stainless steel joints by TIG, laser and laser-TIG hybrid welding', Optics and Lasers in Engineering, Volume 48, Issue 4, pp. 512-517. Available at: https://doi.org/10.1016/j.optlaseng.2009.08.009.

56 Steen, W.M. (1980) 'Arc augmented laser processing of materials', Journal of Applied Physics, 51, pp. 5636–5641. Available at: https://doi.org/10.1063/1.327560.

57 Zuo, W., Ma, L., Lu, Y., Li, S.Y., Ji, Z., & Ding, M. (2018) 'Effects of Solution Treatment Temperatures on Microstructure and Mechanical Properties of TIG–MIG Hybrid Arc Additive Manufactured 5356 Aluminum Alloy', Metals and Materials International, Volume 24, Issue 6, pp. 1346-1358. Available at: https://doi.org/10.1007/s12540-018-0142-3.

58 Zong, R., Chen, J., & Wu, C. (2019) 'A comparison of TIG-MIG hybrid welding with conventional MIG welding in the behaviors of arc, droplet and weld pool', Journal of Materials Processing Technology, Volume 270, pp. 345-355. Available at: https://doi.org/10.1016/j.jmatprotec.2019.03.003.

59 Zhang, Y., Li, Y., Zhang, Y., & Zong, R. (2024) 'Numerical analysis of the behavior of molten pool and the suppression mechanism of undercut defect in TIG-MIG hybrid welding', International Journal of Heat and Mass Transfer, Volume 218, 124757. Available at: https://doi.org/10.1016/j.ijheatmasstransfer.2023.124757.